

Influence of anthropogenic emissions on the composition of highly oxygenated organic molecules in Helsinki: a street canyon and urban background station comparison

Magdalena Okuljar¹, Olga Garmash^{2,5}, Miska Olin², Joni Kalliokoski², Hilkka Timonen³, Jarkko V. Niemi⁴, Pauli Paasonen¹, Jenni Kontkanen^{1,6}, Yanyun Zhang^{1,7}, Heidi Hellén³, Heino Kuuluvainen², Mina Aurela³, Hanna E. Manninen⁴, Mikko Sipilä¹, Topi Rönkkö², Tuukka Petäjä¹, Markku Kulmala¹, Miikka Dal Maso² and Mikael Ehn¹

¹Institute of Atmospheric and Earth System Science, Faculty of Science / Physics, Faculty of Science, University of Helsinki, FI-00014, Helsinki, Finland

²Aerosol Physics Laboratory, Physics Unit, Tampere University, PO Box 692, FI-33014, Tampere, Finland

³Atmospheric Composition Research, Finnish Meteorological Institute, Helsinki, Finland

⁴Helsinki Region Environmental Services Authority, HSY, PO Box 100, FI-00066, Helsinki, Finland

⁵Department of Atmospheric Sciences, University of Washington, Seattle, WA, United States

⁶CSC – IT Center for Science Ltd., Espoo, Finland

⁷University of Lyon, Université Claude Bernard Lyon 1, CNRS, IRCELYON, 69626 Villeurbanne, France

Correspondence to: Magdalena Okuljar (magdalena.okuljar@helsinki.fi)

Abstract. Condensable vapors, including highly oxygenated organic molecules (HOM), govern secondary organic aerosol formation and thereby impact the amount, composition, and properties (e.g. toxicity) of aerosol particles. These vapors are mainly formed in the atmosphere through the oxidation of volatile organic compounds (VOCs). Urban environments contain a variety of VOCs from both anthropogenic and biogenic sources, as well as other species, for instance nitrogen oxides (NO_x), that can greatly influence the formation pathways of condensable vapors like HOM. During the last decade, our understanding of HOM composition and formation has increased dramatically, with most experiments performed in forests or in heavily polluted urban areas. However, studies on the main sources for condensable vapors and secondary organic aerosols (SOA) in biogenically influenced urban areas, such as suburbs or small cities, has been limited. Here, we studied the HOM composition, measured with two nitrate-based chemical ionization mass spectrometers and analyzed using positive matrix factorization (PMF), during late spring at two locations in Helsinki, Finland. Comparing the measured concentrations at a street canyon site and a nearby urban background station, we found a strong influence of NO_x on the HOM formation at both stations, in agreement with previous studies conducted in urban areas. Even though both stations are dominated by anthropogenic VOCs, most of the identified condensable vapors originated from biogenic precursors. This implies that in Helsinki anthropogenic activities mainly influence HOM formation by the effect of NO_x on the biogenic VOC oxidation. At the urban background station, we found condensable vapors formed from two biogenic VOC groups (monoterpenes and sesquiterpenes), while at the street canyon, the only identified biogenic HOM precursor was monoterpenes. At the street canyon, we also observed oxidation products of aliphatic VOCs, which were not observed at the urban background station. The only factors that clearly correlate (temporally and composition-wise) between the two stations contained monoterpene-derived dimers. This suggests that HOM composition and formation mechanisms are strongly dependent on localized emissions and the oxidative environment in these biogenically influenced urban areas, and they can change considerably also within distances of one kilometer within the urban environment. This further suggests that studies should be careful when extrapolating single-point measurements in an urban setting to be representative for district or city scales.

1. Introduction

41 Urban environments can contain various anthropogenic and biogenic sources of volatile organic compounds (VOCs).
42 Biogenic emissions come mostly from urban vegetation, for example, trees and bushes in parks, gardens, and may contain
43 biogenic volatile organic compounds (BVOCs) such as isoprene, monoterpenes (MT), or sesquiterpenes. The sources of
44 anthropogenic emissions consist of traffic, cooking, industrial processes and production of consumer goods, and volatile
45 chemical products (VCP) (Li et al., 2022; Reimann and Lewis, 2007; Watson et al., 2001). Gas-phase compounds emitted
46 from anthropogenic sources contain trace gases, including nitrogen oxides (NO_x), as well as anthropogenic volatile
47 organic compounds (AVOCs), for example aromatic compounds or aliphatic hydrocarbons (Timonen et al., 2017;
48 McDonald et al., 2018). In densely populated areas, VCPs can dominate AVOCs concentrations and compounds typically
49 known as BVOC (e.g., monoterpenes) are also emitted from anthropogenic sources, such as personal care products and
50 cleaning agents (Gkatzelis et al., 2021; Li et al., 2022).

51 Under atmospheric conditions, VOCs can undergo oxidation to form condensable vapors (Pandis et al., 1992; Ehn et al.,
52 2014). The most common ambient oxidants are ozone (O_3), hydroxyl radical (OH), and nitrate radical (NO_3) (Wayne,
53 2000). O_3 is a trace gas produced in the troposphere mostly by photolysis of NO_2 (Liu et al., 1980), and present in the
54 ambient air during the entire day. O_3 can oxidize only VOC containing at least one double or triple bond, or, with a
55 slower reaction rate, carbonyls (Bianchi et al., 2019). OH is a short-lived, highly-reactive compound produced mostly by
56 the photolysis of O_3 (Crutzen et al., 1999), thus OH is present in the atmosphere mainly during the daytime. NO_3 is a
57 product of the reaction between O_3 and NO_2 , which gets rapidly destroyed by photolysis and reactions with NO during
58 the daytime (Wayne et al., 1991). Both radicals can react with most closed-shell VOCs (Seinfeld and Pandis, 2016), but
59 in the atmosphere, NO_3 reacts mostly with alkenes while OH reacts with almost all compounds, including aromatic
60 hydrocarbons (Seinfeld and Pandis, 2016). Oxidation of VOCs almost always leads to peroxy radical (RO_2) intermediates,
61 typically with long enough lifetimes to participate in bimolecular reactions, primarily with NO , HO_2 , or other RO_2 . The
62 RO_2 may also undergo various unimolecular isomerizations, and both these and the bimolecular reactions can lead to
63 either propagation or termination of the organic radical (Bianchi et al., 2019). The structure of the final product depends
64 on multiple factors, including the structure of the initial VOC and the “oxidative conditions”, meaning available oxidants
65 and the bimolecular reaction partners. The latter can be referred to as “terminators” when they terminate the oxidation
66 process, and in some cases the product composition can tell a lot about the oxidative conditions. For example, RO_2
67 termination by NO and oxidation by NO_3 can produce organic nitrogen compounds (ONCs), organonitrates (Atkinson
68 and Arey, 2003; Bianchi et al., 2019), while RO_2 termination by NO_2 can form relatively unstable peroxy nitrates. RO_2
69 cross reactions are the only reactions that can form accretion products, ROOR , referred to here as “dimers” (Valiev et al.,
70 2019).

71 RO_2 intermediates can also undergo autooxidation, where the RO_2 isomerizes through a hydrogen shift (H-shift) creating
72 an alkyl radical to which molecular oxygen can attach (Bianchi et al., 2019; Ehn et al., 2014; Crounse et al., 2013). In the
73 end, a new, more oxidized RO_2 is formed, which can either undergo additional H-shifts or bimolecular reactions, with
74 both potentially terminating or propagating the oxidation (Bianchi et al., 2019) chain. In cases where the radical can
75 undergo multiple autooxidation H-shifts, the end product can reach high enough oxidation levels to be classified as HOM
76 (Bianchi et al., 2019). The structure of a VOC strongly influences its propensity to undergo autooxidation and,
77 consequently, the molar yield of HOM. This results in the very variable HOM yields, which can reach high values for
78 different anthropogenic and biogenic compounds (Molteni et al., 2018; Bianchi et al., 2019; Garmash et al., 2020).
79 Differences in the structural composition affect both the physical and chemical properties of HOM, with more oxidized

80 products typically being less volatile (Kroll and Seinfeld, 2008). However, the exact functionalities are important, and
81 e.g. oxygen atoms in nitrate groups lower the volatility much less than if the oxygen was found in some other functional
82 group (Kroll and Seinfeld, 2008). In general, the high oxygen content of HOM makes them an important contributor to
83 secondary organic aerosol (SOA) formation, influencing e.g. air quality.

84 During the last decade, HOM formation from biogenic emissions have been extensively studied in forests (Ehn et al.,
85 2014; Yan et al., 2016; Bianchi et al., 2017; Massoli et al., 2018), and in agricultural environments (Kürten et al., 2016).
86 Recently, research showed that also the oxidation of AVOCs can noticeably contribute to the HOM population (Molteni
87 et al., 2018; Garmash et al., 2020; Wang et al., 2021) and SOA formation (Timonen et al., 2017). Additionally, NO_x can
88 alter the HOM formation mechanism and influence SOA formation (Fry et al., 2014; Ng et al., 2017; Pullinen et al., 2020;
89 Mutzel et al., 2021). Due to these findings, the research on condensable vapors and their origin focused stronger on urban
90 environments, especially very polluted ones, heavily influenced by anthropogenic emissions (Brean et al., 2019; Liu et
91 al., 2021; Guo et al., 2022b; Nie et al., 2022; Yan et al., 2022). In very polluted environments, formation of condensable
92 vapors is greatly impacted by NO_x (Brean et al., 2019; Liu et al., 2021; Guo et al., 2022b; Nie et al., 2022; Yan et al.,
93 2022) and HOM composition is often dominated by AVOC precursors (Nie et al., 2022).

94 While the composition and formation of condensable vapors have been studied in the above-mentioned forests and highly
95 polluted locations, environments with considerable influence from both anthropogenic and biogenic emission sources
96 have received much less attention. Such areas include urban environments with lots of green areas, for example suburbs,
97 or cities surrounded by large forests. A better understanding of such locations may also help to assess the impact on air
98 quality from adding vegetation such as green roofs to already built-up areas. Helsinki is an example of a city with forests
99 in close proximity, and Saarikoski et al. (2023) estimated that there, even at a street canyon site strongly affected by traffic
100 emissions, BVOCs are the main contributor to oxidation products. While Saarikoski et al. (2023) measured only the
101 composition of VOCs, and not their oxidation products, this finding makes us expect that the relative role of BVOCs is
102 even higher for HOM, as BVOCs typically have higher propensity for autooxidation than AVOC (Bianchi et al., 2019).
103 Another important aspect to consider is the spatial representativeness of typical urban measurements. As cities are very
104 inhomogeneous in terms of local emissions and the oxidative environment, and HOM are short-lived compounds, HOM
105 studies in urban environments that were performed at one specific location may not be comparable to other nearby
106 locations with different urban sub-environments.

107 Here we investigate the composition of condensable vapors at two nearby stations in Helsinki, which are differently
108 influenced by anthropogenic emissions. The first station is located in a busy street canyon while the second is in an urban
109 background area, at less densely built part of Helsinki, 150 meters from the nearest busy road. We studied the composition
110 of condensable vapors, mostly HOM, at these sites using two nitrate-based chemical ionization mass spectrometers. To
111 identify different HOM types from the mass spectra and connect them to different formation pathways, we applied
112 Positive Matrix Factorization (PMF) to separate co-varying species. We compared the drivers of HOM formation between
113 the two urban sub-environments and explored the roles of biogenic and anthropogenic emissions on HOM composition,
114 in order to understand how these can affect the air quality in urban environments with a strong biogenic influence.

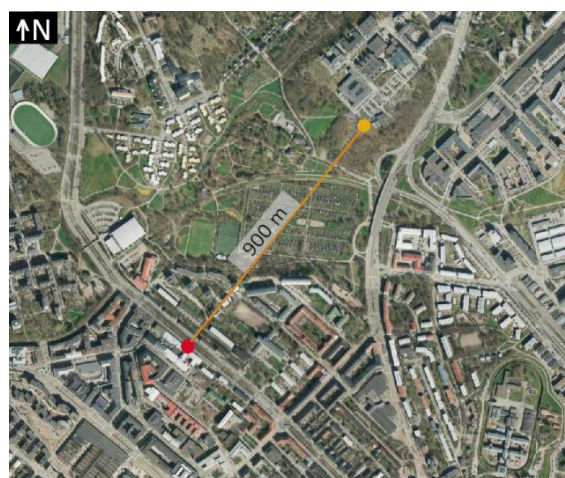
115 2. Methods

116 We measured the composition of condensable vapors at two stations in Helsinki situated in contrasting environments: the
117 Helsinki Region Environmental Services Authority (HSY) air quality station (60°11'47.0'' N, 24°57'07.7'' E) and the

118 Station for Measuring Ecosystem-Atmosphere Relations (SMEAR III, 60°12'10.4'' N, 24°57'40.2'' E) (Fig. 1). The HSY
 119 supersite is located at a street canyon, less than a meter from Mäkeläntie street (around 28 000 vehicles/weekday)
 120 (Kuuluvainen et al., 2018). The street canyon is 42 m wide and the height of buildings on the both sides of the supersite
 121 is 19 and 16 m, leading to the average height-to-width ratio of 0.45 (Järvi et al., 2023). It contains a pavement and three
 122 lines of road for both directions separated by the two tram lines and trees. SMEAR III is 900 m north-east of the HSY
 123 station and with 150 m distance from the closest busy road (Hämeentie street). SMEAR III, is classified as an urban
 124 background station (Järvi et al., 2009). The neighborhood of these stations was previously described in Okuljar et al.
 125 (2021). Here we refer to them as “street canyon” (later also “SC”) and “urban background station” (later also abbreviated
 126 “UB”), respectively.

127 The measurement campaign was conducted during 11 May 2018 – 03 June 2018 at the urban background station and 27
 128 April 2018 – 24 May 2018 at the street canyon. The measurement period was during change of season and by 14 May
 129 2018 the deciduous trees in the surrounding area had fully developed their leaves. To study the influence of traffic
 130 emissions, we analyzed separately the data measured during workdays as well as only during weekends and public
 131 holidays (1 May 2018 and 10 May 2018). We refer to them as ‘workdays’ and ‘weekends’, respectively. As the nighttime
 132 concentrations are often influenced by the emission from the previous day, we separate these categories in 24 h periods
 133 starting at 4 a.m. The corresponding analysis of size distribution of 1-1000 nm particles measured during the same time
 134 at both stations in Helsinki is presented by Okuljar et. al. (2021).

135 The detailed meteorological description of the transport of pollutants at both stations with the emphasis on the mechanism
 136 affecting this transport at the street canyon is presented by Järvi et al. (2023). In summer the atmosphere is very stable
 137 during nighttime and very unstable during daytime at the urban background station. The meteorological conditions at the
 138 urban background station (Fig. 2) resemble the one described by Järvi et al. (2023) for summer, which suggests limited
 139 vertical mixing of the atmosphere during nighttime and very well-mixed lower atmosphere during daytime during our
 140 measurement. At both stations, during the warm period the mechanical and thermal mixing is stronger than during cold
 141 periods resulting in conditions more favorable for pollution dispersion (Järvi et al., 2023). At the street canyon, not only
 142 mean wind but also the turbulent mixing is important for the transport of pollutants. This may suggest that even though
 143 the air is not stagnant, the pollutants are not efficiently transported from the street canyon.



144
 145 Figure 1. Orthophotograph of stations in street canyon (red) and in an urban background environment (yellow) made on
 146 May 7th, 2018. The photograph was provided by The City of Helsinki map service (CC BY 4.0).

2.1. Condensable vapor measurements

The composition of condensable vapors was measured simultaneously at both stations by two nitrate-ion based chemical ionization atmospheric pressure interface (CI-API-TOF) mass spectrometers (MS) (Jokinen et al., 2012). Nitrate ions (NO_3^-), produced by interactions between soft x-ray and sheath air containing nitric acid (HNO_3), binds to the analyzed compound through hydrogen bonds or charges the analyte via proton transfer reactions. NO_3^- is primarily selective towards organic molecules containing at least two suitably positioned hydroxyl (-OH) or hydroperoxyl groups (-OOH) (Hyttinen et al., 2015), or compounds with higher gas-phase acidity than HNO_3 . After the sample gets ionized, the ions are focused in the API module and ultimately separated in the time-of-flight (TOF) analyzer based on their mass-to-charge ratio (m/Q , reported in units of Th). The CI-API-TOF and its working principle was described in detail by Jokinen et al. (2012). The resolving power of the MS at both stations was approximately 3000-4000 Th/Th for signals with m/Q higher than 200 Th. The mass spectra were analyzed using the software package tofTools (Junninen et al., 2010).

In measured mass spectra, we observed multiple peaks at every m/Q . To perform high-resolution (HR) analysis requires us to fit closely set signals and could increase uncertainties of results. Therefore, most of our analysis is based on unit mass resolution (UMR) data and we apply HR analysis at times where PMF indicated low interference to this factor as described in section 2.4. Additionally, we noted that condensable vapor measurement at street canyon had lower transmission for higher m/Q than at urban background station.

Here, we discuss quantitative changes in condensable vapors based on their measured signal in counts per second (cps) normalized by the cps of the reagent ions (NO_3^- , $\text{HNO}_3\text{NO}_3^-$, and $(\text{HNO}_3)_2\text{NO}_3^-$), using the unit ncps (normalized cps). The ambient concentrations can be estimated by using previously determined instrument-specific calibration coefficients for sulfuric acid (Okuljar et al., 2021) equal to $4 \cdot 10^9 \text{ cm}^{-3}$ for the street canyon station and $7 \cdot 10^9 \text{ cm}^{-3}$ for the urban background station. However, usage of these calibration coefficient determined for sulfuric acid to calculate HOM concentration comes with very large uncertainties, and we therefore concentrate on comparison of ion signal strength.

2.2. VOC measurements

VOC concentrations were measured at the street canyon with an offline method in which ambient samples were first collected on a Tenax TA-Carbopack B sorbent tube and later analyzed by thermal desorption gas chromatography coupled with mass spectrometry (TD-GC-MS). We measured VOC concentrations during the period 15 – 25 May 2018 with 4 h time resolution. 13 analytes were classified as AVOCs: benzene, toluene, ethylbenzene, p/m-xylene, styrene, o-xylene, propylbenzene, 3-ethyltoluene, 4-ethyltoluene, 1,3,5-trimethylbenzene, 2-ethyltoluene, 1,2,4-trimethylbenzene, and 1,2,3-trimethylbenzene, and 15 as BVOCs: monoterpenoids (α -pinene, camphene, β -pinene, Δ^3 -carene, p-cymene, 1,8-cineol, limonene, terpinolene), terpene alcohol (linalool), an oxidation product of β -pinene (nopinone), bornyl acetate, and sesquiterpenes (longicyclene, iso-longifolene, β -caryophyllene and α -farnesene). More detailed description of the method can be found e.g. in Helin et al. (2020).

2.3. Other instrumentation

CO_2 , NO, NO_2 , SO_2 as well as meteorological variables were measured at both stations. Table S1 contains information about measurements of additional variables used in this paper.

2.4. Positive Matrix Factorization

183 Collected datasets from the measurement of condensable vapors at both stations consist of an enormous amount of
184 information and it is challenging to filter data that contain relevant information for analysis of HOM formation. As both
185 stations are located in a city, the composition of condensable vapors is dependent on different types of VOC sources as
186 well as chemical and metrological conditions. To extract relevant information, separate different pathways of HOM
187 formation, and find processes affecting condensable vapor composition at both stations, we applied Positive Matrix
188 Factorization (PMF) (Paatero, 1997; Paatero and Tapper, 1994; Paatero and Hopke, 2003). PMF is a multivariate factor
189 analysis model which has been widely used on aerosol mass spectrometry data (Ng et al., 2011; Zhang et al., 2011; Chen
190 et al., 2022) and more recently on ambient gas-phase chemical ionization mass spectrometry data (Yan et al., 2016;
191 Massoli et al., 2018; Zhang et al., 2019; Liu et al., 2021; Nie et al., 2022).

192 We performed PMF analysis on three different m/Q ranges from UMR data at both stations: 200-350 Th, 350-500 Th,
193 and 500-650 Th. In this paper, we will refer to these ranges as ranges 1, 2, and 3, respectively. The loss rate of HOM due
194 to condensation is roughly a function of their mass (Peräkylä et al., 2020), thus, analyzing mass spectra in ranges allows
195 us to group HOM with similar loss rates and focus specifically on separating the HOM sources (Zhang et al., 2020).
196 Additionally, when a m/Q range has lower signal than other ranges, it will only have a minor weight on the PMF solution
197 and relevant information may be lost (Zhang et al., 2020). Using m/Q ranges for PMF analysis is important especially at
198 the street canyon as it may partly counteract the loss of information due to lower transmission for higher m/Q . The focus
199 of our analysis is on compounds in a range of 200 to 650 Th as in this reach we can find majority of the condensable
200 vapors containing C_{5-20} . Smaller m/Q are unlikely to condense, while larger m/Q had very low, or even negligible, signals.
201 We prepared data and error matrices with 30 min time resolution, separately for each range at each station according to
202 the methods described by Yan et al. (2016). To conduct PMF analysis we used the Igor-based interface Source Finder
203 (SoFi, version 6.D) (Canonaco et al., 2013) and ME-2 solver (Paatero, 1999). Detailed information about data preparation
204 and validation of PMF solutions can be found in S1.

205 To describe the chemical composition of ions in obtained factors, we determined the times for each factor when that factor
206 had the highest relative contribution to the total signal and then fit peaks to the HR data to identify the key compounds.
207 Choosing times when the analyte is dominant across all factors in the same m/Q range and at the same site is necessary
208 to ensure that the identified compound is correctly assigned to the factor. In this paper, we performed a more detailed
209 interpretation only of chosen factors from each station, which we refer to further on as “selected factors”. A factor was
210 chosen for further interpretation only when we could reasonably identify ions in it, and relate it to a real atmospheric
211 source, i.e. not impurities. We refer to other factors as “not selected factors”. Examples of each type will be given later to
212 better clarify this selection process.

213 2.5. Limitation of data for interpretation

214 There are several limitations for interpreting the data. At the street canyon, a low signal is observed for higher m/Q . That
215 leads to a low signal-to-noise ratio (S/N) for HOM measured in range 2 and 3, and in some cases makes it impossible to
216 identify the compounds. As a result of fast decrease of measured signal with an increase of m/Q , at the street canyon, over
217 90 % of the signal of 200-650 Th is located in range 1. This could be caused by a lower transmission for high m/Q of the
218 CI-API-TOF measurement at that station. Transmission is a result of voltage settings in CI-API-TOF, which are optimized
219 for each instrument separately. We could not correct our data for transmission. Zha et al. (2018) showed that the ratio of
220 the signal for the same sampled air measured by two CI-API-TOF can change drastically with an increase of m/Q due to
221 the difference in the transmission between instruments. Thus, the highest uncertainty caused by inconsistent transmission

222 between two instruments is observed in range 3. Nevertheless, this uncertainty does not influence identification of peaks
223 that have sufficient S/N.

224 Due to the chemical complexity of the samples, we cannot achieve high accuracy of mass calibration on some of the
225 measured days. This is the reason why we have performed PMF analysis on UMR data. Limitations of peak identification
226 due to the MS resolution and the presence of multiple overlapping peaks also hinder the identification of some ions, and
227 hence we are confident to report only the dominant ions in each factor. We are not able to report key compounds for
228 factors that have minor contribution to their m/Q range or have too many similar peaks with other factors, as we cannot
229 unambiguously assign identified compounds to these specific factors.

230 Lastly, we need to keep in mind that chemical ionization with NO_3^- is very selective, mostly towards highly functionalized
231 compounds. Overall, this ionization method is optimal for detection of HOM, however, it limits observations of other
232 oxidation products.

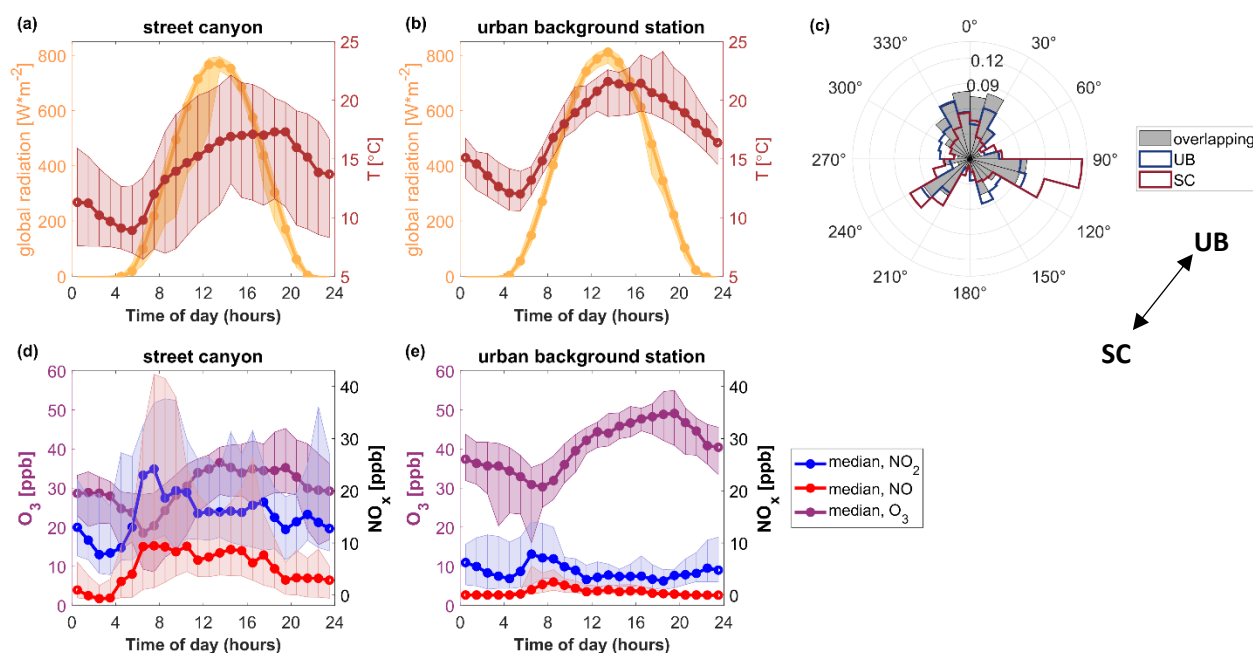
233 3. Results and discussion

234 We start this section by providing a short overview of the meteorological conditions during the campaign. In section 3.2,
235 we present our main findings, starting from the PMF results and the subsequent interpretations of important formation
236 pathways of condensable vapors at the two measurement sites. In the last part of this section, we discuss the potential
237 implications of our findings on the air quality in Helsinki.

238 Concerning notations, we focus our study on HOM, but we also detect abundant organic compounds which contain less
239 than six oxygen atoms, which do not classify as HOM. Thus, we often use a broader term ‘condensable vapors’ when
240 discussing observed products more broadly. In addition, we observe monomeric (mostly $\text{C}_9\text{-C}_{10}$) and dimeric (mostly $\text{C}_{19}\text{-}$
241 C_{20}) oxidation products of MT, which we refer to as ‘MT-derived monomers’ and ‘MT-derived dimers’, respectively. For
242 simplicity, we call factors containing monomeric oxidation products of MT ‘MT monomers’ while ‘MT dimers’ factors
243 contain dimeric oxidation products of MT.

244 3.1. Overview of meteorological and trace gas conditions in Helsinki

245 Atmospheric conditions, for example local emissions and oxidative environment, influence HOM formation pathways.
246 To understand HOM formation mechanisms and their differences between studied sites, we first investigated
247 meteorological and chemical conditions at both stations. Figure 2 presents diurnal variations of measured variables that
248 can influence HOM formation pathways: global radiation, ambient temperature (T), and concentrations of O_3 , NO, and
249 NO_2 as well as the wind direction measured during this campaign. As mentioned earlier, the measurement periods
250 overlapped but were not identical between the two stations. Therefore, differences in campaign averages between sites
251 are partly driven by differences in location and partly by differences in time. The difference in meteorological parameters
252 (ambient temperature, global radiation, wind direction) are driven mostly by changes in the measurement period (Fig. 2,
253 S2), while the trace gases (NO, NO_2 , O_3) vary largely also during overlapping times of measurements (11 May 2018 – 24
254 May 2018) (Fig. S2).



255

256 Figure 2. Diurnal variations of (a,b) global radiation and ambient temperature, and (d,e) NO , NO_2 , and O_3 concentrations
 257 at the street canyon (left) and urban background station (middle). The median diurnal variations are shown as solid lines
 258 with markers; 25th to 75th percentile ranges are presented as shaded areas. Time is local. The right panel (c) shows a wind
 259 rose for the overlapping time at both stations as well as outline of wind rose for the period when data was collected from
 260 the street canyon (SC, dark red) and the urban background station (UB, dark blue). Arrow in panel (c) shows the direction
 261 of the urban background station (UB) in relation to the street canyon (SC). Presented data contain both workdays and
 262 weekends.

263 Diurnal variation of global radiation is similar between the two stations (Figure 2 a,b), though with slightly more cloudy
 264 periods at the street canyon. Global radiation initiates photolysis reactions and, as a result, enhances the formation of OH
 265 and O_3 as well as the decomposition of NO_3 . During the overlapping time of measurements, the urban background station
 266 was more likely to be the downwind station, however the wind was mostly coming from North (Fig. 2c), meaning that
 267 neither station would receive emissions from the other. Median temperatures varied between 12.0 $^{\circ}\text{C}$ and 21.6 $^{\circ}\text{C}$ at the
 268 urban background site and between 8.9 $^{\circ}\text{C}$ and 17.3 $^{\circ}\text{C}$ in the street canyon. Higher temperature at the urban background
 269 station can be explained by the difference in measurement periods as the measurements started two weeks later than in
 270 street canyon. During the period when measurements overlapped, the median temperature is very similar between stations
 271 reaching almost 22 $^{\circ}\text{C}$ during daytime and dropping to 12-13.4 $^{\circ}\text{C}$ during nighttime (Fig. S2). The increase in temperature
 272 typically accelerates molecular reaction rates as well as enhances BVOCs emissions and evaporation rates. It can also
 273 affect HOM yields (Quelever et al., 2019).

274 At the urban background station, NO has a maximum between 8:00 and 9:00 (2.5 ppb) and it is negligible during
 275 nighttime. In contrast, at the street canyon, the median NO concentration was below the detection limit between 1:00 and
 276 3:00, after which it rapidly increased, levelling off at 7:00 and staying elevated (ca. 9 ppb) throughout the day until 17:00.
 277 That means NO can affect oxidation reactions more at the street canyon site, even during much of the night, when it stays
 278 at 4 ppb until early morning. In the context of VOC oxidation, the presence of NO likely causes the termination of the
 279 oxidation. In the absence of NO , termination reactions with RO_2 become more favorable. NO_2 and NO (Figure 2 c,d)

concentrations are up to 5 and 23 times higher at the street canyon than at the urban background station, respectively. At urban background site, O₃ reaches minimum median concentration at 7:00 (30.3 ppb) and maximum at 19:00 (49.1 ppb). At the street canyon, the corresponding values are 18.5 ppb at 6:00 and 36.5 ppb at 13:00. During overlapping times between the sites, median O₃ concentration stays 5-25 ppb lower at street canyon than at urban background station (Fig. S2). It could be partly associated with higher NO concentration in street canyon as NO reacts with O₃. O₃ remains relevant for VOCs oxidation throughout the day. O₃ and NO₂ concentrations affect production of NO₃ and thus its concentration.

3.2. Characterization of PMF factors

In this subsection, we examine the HOM composition and formation at both stations by investigating PMF factors in all three m/Q ranges (200-350 Th, 350-500 Th, 500-650 Th); we focus our analysis on selected factors, their time-series (Fig. S3-4), and diurnal variations (Fig. 3-4) as well as mass spectra (Fig. S5-6). We refer to PMF factors as SCX-Y or UBX-Y where SC is the street canyon, UB is the urban background station, X is the analyzed m/Q range (either 1, 2, or 3), and Y is the identifying number of the factor in that range. The factors also appear together with a descriptive name. As an example, “UB3-2: MT dimers” refers to the second PMF factor identified in mass range 3 at the urban background site and was found to mainly contain ions related to monoterpene-derived dimers. To understand the chemical composition of factors, we identify their key compounds with HR data (Table S2) as described in Sect. 2.5. All key compounds are detected as clusters with NO₃⁻ or HNO₃NO₃⁻ and this is how we report them in Table S2 and on the mass spectra (Fig. S5-6 and S9-10); however, for clarity of the interpretation in this subsection, we write their chemical structures without the nitrate adducts.

In this subsection, we summarize the key characteristics give an interpretation of factors. The more detail description of the PMF analysis can be found in the supplementary information (SI) (S2. PMF inputs and validation, S4. Factor interpretation). Only “selected” factors are described here, while characteristics of “not selected” factors are presented and described in the SI (Sect. S4, Fig. S9-10, Table S3). Several reasons motivated us not to select factors for detailed discussion in the main text. For example, a factor was not selected if it was a contamination or an artefact (e.g., containing mainly water clusters isotopes) or if we were not confident in the meaningful separation of this factor by PMF method (this was the case for the entire range 1 at the street canyon, as described below). Overall, we selected 5 out of 13 factors from the street canyon and 10 out of 14 factors from the urban background station. These selected factors explain 34%, 100%, and 100% of the observed signal in ranges 1-3 at the urban background station and 0%, 64%, and 61% of the observed signal in ranges 1-3 at the street canyon, respectively (Table 1, Fig. S7-8).

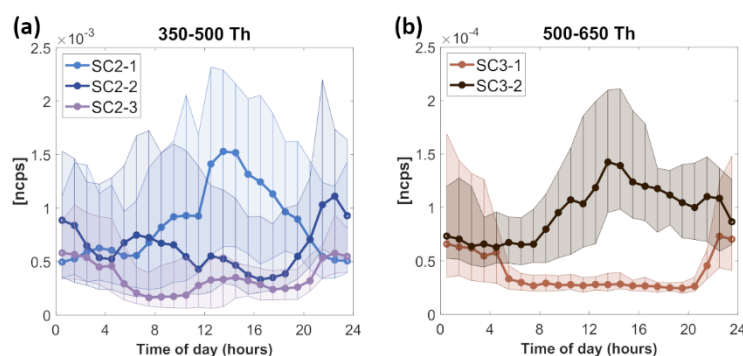


Figure 3. The diurnal variation of PMF factors fractions at the street canyon (SC). PMF factors are labeled as SCX-Y where X stands for the analyzed m/Q range (2 or 3), and Y is the identifying number of the factor in that range. The median diurnal variation is shown as a solid line with markers; 25th to 75th percentile ranges are presented as shaded areas. Y-axis in ncps indicates the measured signal in normalized counts per second.

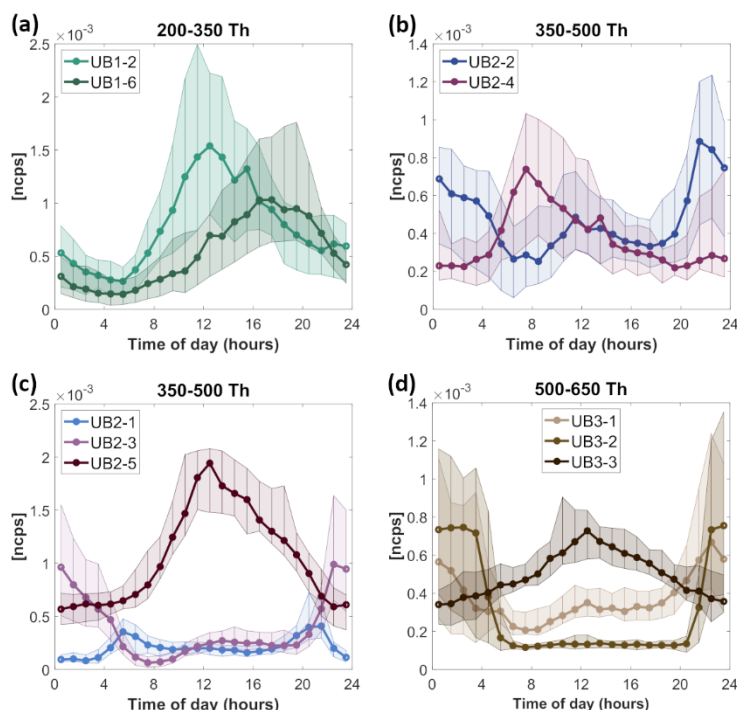


Figure 4. The diurnal variation of PMF factors at the urban background station (UB). PMF factors are labeled as UBX-Y where X stands for the analyzed m/Q range (1, 2, or 3), and Y is the identifying number of the factor in that range. The median diurnal variation is shown as a solid line with markers; the 25th and 75th percentile ranges are presented as shaded areas. Y-axis in ncps indicates the measured signal in normalized counts per second.

3.2.1. Street canyon

Here, we very briefly describe factors observed at the street canyon site in each m/Q range. The main examination of the factors is given in Sect. 3.2.3 where we also discuss them in relation to factors observed at the urban background station. As indicated already above, PMF solutions for range 1 at the street canyon were inconclusive, and therefore all factors from this range are classified as ‘not selected’. The main reason is that all factors had very similar temporal trends, mainly correlating with temperature. This may be a result of most observed molecules being semi-volatile, and increased temperatures lead to increased evaporation of these molecules. In any case, as PMF relies on temporal variability to separate factors, too much co-variance makes PMF less reliable. Nevertheless, we believe there was some useful information also in this range and will briefly discuss *SCI-1: nitrophenol 1*, *SCI-2: MT monomers 3*, and *SCI-5: nitrophenol & aliphatic* in this section.

Range 1, 200-350 Th (Factors selected: 0/5)

In range 1, all factors are affected by changes in ambient temperature (Fig. S9 and S13). Factors in range 1 have a daytime peak and nearly all of them could have been oxidized by OH or O₃ (Fig. S9, Table S3). Most of these factors are likely

332 formed from AVOCs and contain nitrophenol ($C_6H_5O_3N$) as well as other N-containing aromatics, such as nitroresol.
333 Nitrophenol can be directly emitted from combustion or formed from benzene and phenol oxidation. The presence of
334 nitrophenol in many factors can be explained by an abundance of benzene at the street canyon as it is the third most
335 abundant VOC measured at the street canyon site (Fig. S11).

336 **Range 2, 350-500 Th (Factors selected: 3/5)**

337 In range 2, all selected factors respond to the changes in the ambient temperature (Fig. S3 and S13), especially factor
338 SC2-1, which contains monomeric oxidation products of MT (MT-derived monomers) with nitrate functionalities
339 ($C_{10}H_{16}O_{8-10}N_{0-2}$ and/or $C_9H_{14,16}O_{9-10}N_2$). Factors SC2-2 and SC2-3 are highest during the night, but they also have local
340 maxima during the day, which suggests that competing processes influence the formation of these factors and thus their
341 diurnal pattern. SC2-3 may be inhibited by NO, as it decreases when NO reaches its daily maximum (Figure 3d). SC2-3
342 consists of MT-derived monomers ($C_{10}H_{16}O_{10-11}N_2$ and $C_{10}H_{16}O_{10}$), while SC2-2 is dominated by one single compound:
343 $C_{10}H_{16}O_9N_2$.

344 **Range 3, 500-650 Th (Factors selected: 2/3)**

345 Range 3 contains one daytime and one nighttime factor. SC3-1 is a MT-derived dimer factor produced via oxidation by
346 NO_3 and present during the night, when NO concentrations are low enough to allow RO_2 termination via RO_2 cross
347 reactions. The key compounds detected in SC3-1 are coming from one oxidation chain: $C_{20}H_{32}O_{11-15}N_2$. SC3-2 is a
348 daytime factor containing HOM oxidized by OH ($C_{19}H_{22,24}O_{10}N_2$). SC3-2 also has some signal from instrumental
349 impurities containing fluorine (F-impurities), and undefined noise peaks.

350 **3.2.2. Urban background station**

351 Similar to the previous subsection, we describe briefly factors observed in all ranges at the urban background station.
352 The discussion about these factors follows in Sect. 3.2.3, in which we compare factors found at both sites in Helsinki.

353 **Range 1, 200-350 Th (Factors selected: 2/6)**

354 Selected factors in range 1 contain daytime factors, from which UB1-6 is a factor correlating the best with the ambient
355 temperature (Fig. S4 and S14). Time-series of UB1-6 correlates with O_3 (Fig 4a, Fig. S14) and it contains key compounds
356 with C_{7-8} atoms. These formulas have been detected earlier as products of MT oxidation in chamber studies (Yan et al.,
357 2020) and in ambient measurement (Liu et al., 2021), however, they have also been identified as oxidation products of
358 aromatic VOCs (Guo et al., 2022b). Since CI-API-TOF does not provide information about molecular structure, we cannot
359 unambiguously determine the origin of this factor. In contrast to UB1-6, UB1-2 factor contains nitrophenol and likely
360 originates from AVOCs. The diurnal variation of UB1-2 resembles the one expected for OH (Saarikoski et al., 2023).
361 Both UB1-2 and UB1-6 contain ONCs and their oxidation was likely terminated by NO or NO_2 .

362 **Range 2, 350-500 Th (Factors selected: 5/5)**

363 Range 2 contains various daytime and nighttime factors (Fig. 4). Factor UB2-1 reaches the highest concentrations at 5
364 am. and 10 pm., which corresponds to the time of sunrise and sunset during our measurement period. As this factor
365 consists of MT-derived ONCs, possibly with at least two N-atoms ($C_9H_{14}O_{9,11}N_2$ or $C_{10}H_{16}O_{9,11}N$, and $C_{10}H_{17}O_{12}N_3$), we
366 can speculate that they are formed from NO_3 oxidation of MT and terminated by NO. Chamber experiments have shown
367 that formation of condensable vapors through NO_3 oxidation and NO termination is a possible formation mechanism

during NO_x-influenced oxidation of monoterpenes (Yan et al., 2020; Nie et al., 2023). It is typically assumed that NO₃ and NO would not co-exist in the atmosphere. However, in urban areas NO concentration is not negligible during the night and this pathway was previously suggested as possible mechanism of ONC formation in Beijing (Guo et al., 2022b). Simultaneous presence of NO₃ and NO when photolysis is just high enough to form NO but not to fully deplete NO₃ is a plausible explanation for the diurnal pattern of UB2-1.

UB2-2 and UB2-3 are both nighttime factors oxidized mainly by NO₃ and inhibited by NO during daytime. UB2-2 contains MT-derived monomers and correlates with the MT-derived dimer factor (UB3-2). Following the diurnal cycle in Fig. 4b, it can be observed that when the concentration of UB2-2 decreases, the concentration of daytime MT-derived monomer factor, UB2-4, increases. Even though UB2-2 and UB2-4 both contain key compounds with C₉₋₁₀, the molecular formulas are slightly different. Specifically, in UB2-2 key compounds contain mainly one or three N-atoms while in UB2-4 they have mostly zero or two N-atoms (Table S2). UB2-2 and UB2-4 could thus be formed from competing HOM formation pathways from the same VOCs.

In contrast to other factors, UB2-3 consists of HOM with composition of C₁₅H₂₃O_{8,10,12-13}N, based on which we conclude that this factor is formed from sesquiterpenes (C₁₅H₂₄, Richters et al., 2016). UB2-3 correlates very well with a corresponding sesquiterpene factor from range 3, UB3-1 (R=0.93) (Fig. S12). The last factor UB2-5 is a daytime factor which during noon corresponds to more than 50% of the measured signal (Fig. S8). It contains C₁₀ compounds (C₁₀H₁₁O₉N and C₁₀H₁₆O₉N₂) and most likely that UB2-5 is formed in OH oxidation.

Range 3, 500-650 Th (Factors selected: 3/3)

Range 3 at UB site contains two nighttime factors: sesquiterpene-derived UB3-1 factor (C₁₅H₂₃O₁₀₋₁₃N and C₁₅H₂₃O₁₄₋₁₆N (or C₁₅H₂₄O₁₃₋₁₆N₂)), and MT-derived dimer UB3-2 factor (mostly containing C₂₀ compounds, for example C₂₀H₃₂O₁₃₋₁₆N₂). Both factors consist of ONCs, products of NO₃ oxidation of BVOCs, and are inhibited by NO, being absent during the day as a result. UB3-3 is the only daytime factor (Fig. 4d) in range 3 and it consists of OH-oxidized HOM, F-impurities, and noise.

3.2.3. Factor interpretation and comparison between urban background and street canyon sites

Tables 1 and S3 present the most plausible interpretation of selected and not selected factors, respectively. For each factor, we propose VOC precursors, oxidants, and terminators, which were most likely to influence the formation of species in this factor. We also specify an hour of the day when factor's signal reached its maximum as well as the contribution of this factor to the total signal both within its own m/Q sub-range and within the full analyzed range (200-650 Th). See Table 1 caption for a more detailed description of how to read the table. The findings and implications are discussed below. While discussing time series correlations between factors from both stations, it is important to keep in mind that they cannot be ideal. We estimated that the highest correlation between stations for condensable vapors is approx. 0.88 which is a correlation between concentrations of a compound that is mostly produced in the same pathway on both sites: sulfuric acid (SA) (Fig. S15).

Table 1. Suggested characterization of selected factors at both stations. Detailed factor interpretation is described in Sect. S3. The importance of the various species described in this table was assessed based on either factor time series (TS), factor mass spectra (MS), or both (B), as indicated by the superscript in the “Factor” column. The “Precursor” column describes which type of molecules we expect to act as precursors to the observed signals, separating (when possible) between AVOC and BVOC. The “Oxidant” and “Terminator” columns depict our estimates for the most likely species involved in the oxidation process (“M”, as in “maybe”, is used if we were unable to exclude or confirm the participation of the species). If the “yes” or “no” is marked in bold font, it means that we found a particularly clear influence of that species for that factor. The “Diurnal peak time” shows the hour when the factor had its highest concentration, and “Fraction” depicts the percentage of signal (of the given sub-range or the total analyzed m/Q range) that the factor contributed to.

Range [Th]	Factor	Precursor	Oxidant			Terminator			Diurnal peak time	Fraction [%] within	
			OH	NO ₃	O ₃	NO	RO ₂	HO ₂		200-650	sub- range
Street canyon											
350-500	SC2-1 ^{TS}	BVOCs	M	no	M	yes	no	M	13	2.2	27.2
	SC2-2 ^{TS}	VOCs	no	yes	M	M	no	M	22	2.0	24.8
	SC2-3 ^{TS}	BVOCs	no	yes	no	no	M	M	0	0.9	11.5
500-650	SC3-1 ^B	BVOCs	no	yes	no	no	yes	no	22	0.1	19.3
	SC3-2 ^{MS}	VOCs, noise, F-impurities	yes	no	M	yes	no	M	13	0.2	41.6
Urban background station											
200-350	UB1-2 ^{MS}	AVOCs	yes	no	no	yes	no	M	12	8.9	16.1
	UB1-6 ^{TS}	VOCs	M	no	M	yes	no	M	17	7.4	17.8
	UB2-1 ^{TS}	BVOCs	no	yes	no	yes	no	M	21	2.6	8.6
350-500	UB2-2 ^{TS}	BVOCs	no	yes	M	no	M	M	21	5.4	18.0
	UB2-3 ^{MS}	BVOCs	no	yes	M	no	no	M	22	5.1	17.0
	UB2-4 ^{TS}	BVOCs	M	no	M	yes	no	M	7	4.9	16.5
500-650	UB2-5 ^{MS}	VOCs, noise	yes	no	M	yes	no	M	12	12.0	39.9
	UB3-1 ^B	BVOCs	no	yes	M	no	no	M	22	4.9	34.3
	UB3-2 ^B	BVOCs	no	yes	M	no	yes	no	23	3.6	25.4
	UB3-3 ^{MS}	VOCs, noise	yes	no	no	yes	no	M	12	5.6	40.3

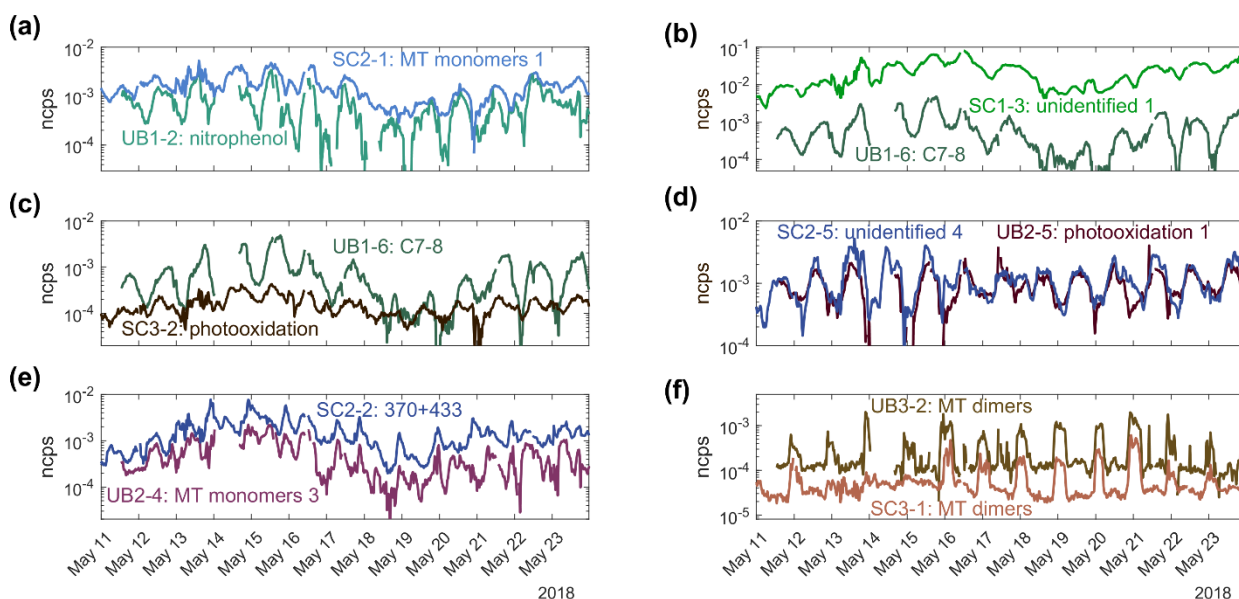


Figure 5. Time series of PMF factors with Pearson correlation coefficient higher than 0.7 (Figure S12) between the street canyon (SC) and the urban background station (UB) for common measurement time. PMF factors are labeled as SCX-Y or UBX-Y where X stands for the analyzed m/Q range (1, 2, or 3), and Y is the identifying number of the factor in that range.

The total concentration of AVOCs is much higher than BVOCs at both stations (shown for street canyon in Fig. S11), however, most of the selected factors are more likely to have biogenic origin, primarily based on the identified peaks in the mass spectra (Table 1, Sect. S4). Our result is in agreement with the earlier study by Saarikoski et al. (2023) which concluded that, despite dominant AVOCs concentrations at street canyon site, BVOCs are estimated to be the main source of oxidized products, due to their higher reactivities. MT are the only type of biogenic precursors identified at the street canyon while at the urban background station we find oxidation products of both MT and sesquiterpenes. This is likely due to the difference in proximity of trees and vegetation from the stations as none of measured sesquiterpenes exceeded 0.2% of measured total BVOC concentrations at the street canyon. All key compounds detected in MT-derived factors were previously reported in studies investigating the influence of NO_x on HOM formation from MT precursors (Pullinen et al., 2020; Yan et al., 2020; Shen et al., 2021; Dam et al., 2022; Guo et al., 2022a). MT can be also emitted from anthropogenic sources, for instance in form of VCPs (Gkatzelis et al., 2021; Li et al., 2022). VCPs are known to be very important emitters (Karl et al., 2018); however, based on our results, it seems that the concentrations of biogenic terpenes are the main contributor to the formation of organic condensable vapors. This is because the population density of Helsinki is low enough that the VCP-emitted MT signature is likely lost among the abundant biogenic MT signals. Additionally, it is probable that the biogenic terpenes to a large extent transported into Helsinki from more rural areas, but also emissions of biogenic terpenes within Helsinki can be important, as has been shown to be the case in various cities (Kota et al., 2014; Kaltsonoudis et al., 2016; Rantala et al., 2016; Kaser et al., 2022). This is in agreement with α -pinene being the most abundant BVOC and a common VCP-emitted MT, limonene (Coggon et al., 2021), being very low (<5% of BVOC concentration).

We observed only few PMF factors that we expect to originate from AVOC oxidation, and for both stations AVOC factors are detected only for the smallest m/Q sub-range, 200-350 Th (Table 1, Table S3). None of the factors had diurnal variations resembling traffic emissions at these sites (Olin et al., 2020; Okuljar et al., 2021). Even though concentrations

of some factors differed between weekends and workdays, the diurnal behavior of factors was very similar (Fig. S16-17). This suggests that the local emissions from traffic at these sites did not oxidize fast enough, and with high enough yields of detectable compounds, to considerably contribute to our measured signals. This is in line with conclusions presented by Brean et al. (2019) and Saarikoski et al. (2023). As precursor VOC concentrations are also affected by the mixing layer height (MLH), this effect may also impact HOM formation. However, VOCs are only one of the components that affect HOM formation, the effect of the MLH on HOM observed in this study is expected to be small.

Between the two stations, there are only a few factors with similar key compounds (Table S2). *SC3-1: MT dimers* has partly corresponding key compounds with *UB3-2: MT dimers*. They both contain $C_{20}H_{32}O_xN_2$ compounds, where x is 11-15 for SC and 13-16 for UB. *UB3-2: MT dimers* contains also other types of dimers which are not usually present in *SC3-1: MT dimers*. These slight differences between stations may be caused by the small difference in concentration of oxidant, or the concentration or type of MT. The non-negligible concentration of NO during nighttime at SC may also impact the dimer formation there. Nevertheless, these factors are very similar and form through similar pathways (Table 1) – oxidation of MT mostly by NO_3 , and termination through RO_2 cross reactions, leading also to correlating time series ($R=0.77$, Fig. 5 and S12). The $RO_2 + RO_2$ reactions forming the MT-derived dimers will inevitably also form monomers as the dimer yield is never 100 %. However, monomers can also form through all other RO_2 termination channels, making them much more heterogeneous than the dimers. The time evolution of some MT-derived monomer factor time series (*SC2-3: MT monomers 2* and *UB2-2: MT monomers 2*) correlate with the corresponding dimer factors ($R=0.7$ and $R=0.67$ respectively) as well as with each other ($R=0.57$). While both factors are dominated by C_{10} compounds, their detailed mass spectra have significant differences (Fig. S5 and S6): *UB2-2: MT monomers 2* contains mainly ONCs with one N-atom while *SC2-3: MT monomers 2* has more compounds with two N-atoms (Table S2). This may indicate that there is enough NO available to terminate some fraction of the RO_2 , yet without totally shutting down the $RO_2 + RO_2$ channel.

Another pair of factors showing similarities between the stations is *SC2-2: 370+433* and *UB2-4: MT monomers 3* (Fig. 5). Both factors are driven mostly by one compound ($C_{10}H_{16}O_9N_2$), which has been detected as two clusters $C_{10}H_{16}O_9N_2 \cdot NO_3^-$ (370 Th) and $C_{10}H_{16}O_9N_2 \cdot HNO_3 \cdot NO_3^-$ (433 Th) in our instrument (determined by correlation analysis). The high time series correlation ($R=0.75$) suggests that molecules in these factors are formed via very similar pathways between the sites. Potentially, the formation pathways are identical, but importance of some competing pathways differ between the sites. Overall, the lack of stronger resemblance between these nearby sites suggests that even if HOM have the same VOC precursors, the environmental conditions regulate the relative importance between different oxidation pathways.

While differences in emissions and oxidation reactions will lead to diverse mass spectra, also the time series are expected to vary between the sites as the wind direction changes. For example, the street canyon site will likely be impacted by the street in different ways if the wind direction is from the street or towards the street. A clearly longer campaign than ours would be needed to identify the detailed impacts from different wind directions. However, analysis of the average diurnal variation can help us understand the roles of different oxidation conditions if the impact of varying wind directions diminishes in a longer average. Most factors at both stations can be characterized by one of a few types of diurnal patterns. Factors with a daytime diurnal variation reaching maximum concentration during noon or afternoon resemble diurnal variation of OH or O_3 , respectively. However, temperature also peaks in the afternoon, and can lead to both higher BVOC emissions as well as evaporation of semi-volatile species from aerosols or surfaces, convoluting the effect of the oxidants on the observed HOM. Factors with noon or afternoon maxima are mostly found in range 1 at both sites. As range 1

478 mostly contains species thought to be semi-volatile (Peräkylä et al., 2020), it is possible that much of the observed
479 variation is indeed due to the higher temperature causing increased partitioning of these compounds into the gas phase.
480 Nevertheless, OH and O₃ are likely involved as well, and given that the vast majority of signals are ONCs, RO₂
481 termination by NO is to be expected for most species. The opposite can be said for nighttime factors, which are likely
482 inhibited in the daytime by NO, as their formation involves RO₂ termination via other pathways. This becomes especially
483 visible for HOM terminated via RO₂ + RO₂ reactions (Ehn et al., 2014; Yan et al., 2016), which are mainly present in
484 range 3. In this range, the volatilities are overwhelmingly low or extremely low, meaning that ambient temperature
485 changes will not impact their ability to condense irreversibly to aerosols, thus also making their temporal behavior easier
486 to interpret.

487 While daytime and nighttime peaks can be explained quite straightforwardly through variations in temperature or
488 available oxidants or terminators that all follow distinct diurnal trends, we also observed additional types of diurnal trends,
489 present mostly in range 2. Factor *UB2-1: Monoterpenes 1* had a peak in morning and evening (Fig. 4), around sunrise and
490 sunset. We can speculate that these are the periods when sunlight was still available, but at limited amounts. This effect
491 may cause an optimal situation for having both NO₃ and NO participating in the oxidation process. This is supported by
492 the high N-atom content of the main species in this factor. Meanwhile, some other factors showed an opposite trend to
493 UB2-1, namely minima during morning and evening, often with a strong nighttime peak and a smaller daytime increase.
494 Some of the most prominent factors with such behavior were *SC2-3: MT monomers 2*, *UB2-2: MT monomers 2*, *UB2-3:*
495 *sesquiterpene 1*, and *UB3-1: sesquiterpene 2*. NO₃ was identified as the main oxidant for these factors based on the mass
496 spectra and the high nighttime signals, but the local maxima around noon is surprising. Saarikoski et al. (2023) did
497 estimate that NO₃ would have a small daytime maximum, likely due to the sinks not being fast enough to fully overwhelm
498 the very high formation rates from high O₃ and NO₂ during this time. We cannot determine to which extent the diurnal
499 variation of NO₃ influences these diurnal patterns. As was the case also in many situations discussed above, we are often
500 unable to separate if an increase is due to an enhanced source strength or a decrease in competing reaction pathways.

501 **Comparison to previous research**

502 HOM data from Helsinki show similarities with previous studies done on ambient HOM data in urban as well as rural
503 environments. Yan et al. (2016) investigated HOM formation pathways at a boreal forest site (SMEAR II station, Hyytiälä,
504 Finland) located approximately 190 km from Helsinki and 50 km from the closest city – Tampere (with population
505 approximately 250 000). A factor “*Nighttype type-2*”, obtained from PMF analysis by Yan et al. (2016) contained MT-
506 derived dimers formed by NO₃ and O₃ oxidation and RO₂ termination. That factor mostly consisted of C₂₀H₃₁O₁₀₋₁₈N
507 (40%) and C₂₀H₃₂O₁₀₋₁₇N₂ (20%) suggesting that the dimers detected in Hyytiälä and in Helsinki (both stations) have the
508 same formation pathways, even though these measurement sites represent different rural and urban environment. Despite
509 relatively similar precursors and formation pathways, far fewer similarities are found between the mass spectra of MT-
510 derived monomer factors at these three sites. This suggests, as also mentioned above, that monomer formation pathways
511 are much more diverse compared to dimer formation. Still, a comparison of our results with other studies done in rural
512 environments (Massoli et al., 2018; Kürten et al., 2016) showed clearly lower resemblance between MT-derived dimers
513 than one described in preceding sentences, which is likely a result of different biome types in their studies (isoprene-
514 dominated south east US and rural agricultural site in Germany respectively) compared the ones conducted in Finland.

515 In recent years, more research on condensable vapor formation has been conducted in urban environments heavily
516 influenced by NO_x (Yan et al., 2022; Guo et al., 2022b; Liu et al., 2021; Nie et al., 2022; Zhang et al., 2022). Unlike forest

environments, where the fraction of nitrogen-containing HOM is similar to the fraction of HOM without nitrogen atoms (Yan et al., 2016; Massoli et al., 2018), condensable vapor composition in Chinese megacities is dominated by nitrogen-containing compounds, which represent approximately 60-85% of all measured condensable vapors (Guo et al., 2022b; Liu et al., 2021; Nie et al., 2022; Zhang et al., 2022). This strong influence by NO_x was also observed in the present study at both stations in Helsinki. In addition, the majority of key compounds in *SCI-5: nitrophenol & aliphatic* are also listed as main compounds in factors originating from aliphatic AVOCs detected in Nanjing (*Aliph-OOM*) (Liu et al., 2021) and in Beijing (*aliphatic OOMs*) (Guo et al., 2022b). However, depending on the time of the year, the main precursors for condensable vapors in cities in China are either AVOCs or a mix of AVOCs and BVOCs (Guo et al., 2022b; Liu et al., 2021; Nie et al., 2022). During spring, 77 % of all measured condensable vapors originate from AVOC in Beijing (Guo et al., 2022b). This is different compared to Helsinki, where BVOC-derived vapors were more abundant. This dissimilarity is likely due to the AVOC:BVOC ratio being much larger in Chinese cities due to closer proximity of much larger areas with anthropogenic emissions. In contrast, Helsinki AVOC:BVOC is much smaller due to larger BVOC emissions from abundant vegetation in the close surroundings. It is also important to notice that most studies of condensable vapors in Chinese cities (Guo et al., 2022b; Liu et al., 2021; Nie et al., 2022) analyzed much smaller mass range (200-400 Th or 250-400 Th), which corresponds to range 1-2 here. In our study, range 1 is the only mass range in which we find the dominant influence of anthropogenic precursors. Brean et al. (2019) also showed that MT-derived dimer concentrations were approximately 50 times lower than MT-derived monomers in Beijing, likely due to both small MT emissions and suppression of dimer formation by NO.

3.3. Implications for air quality

Ambient air pollution was recognized as the largest environmental health risk and one of the top risk factors for the loss of healthy years (Lim et al., 2012; Anderson et al., 2012; Cohen et al., 2017). Premature deaths caused by ambient air pollution are linked to particulate matter (PM) (Cohen et al., 2017; WHO, 2021), both due to short-term (Pope and Dockery, 2012) and long-term exposure (Burnett et al., 2014). In many environments, including different urban areas, PM is dominated by secondary aerosol formed from condensable vapors, including HOM. HOM and other condensable organic vapors impact not only PM concentration but also the chemical composition of SOA and, consequently, aerosol properties like toxicity. For example, in a recent study with human alveolar epithelial cells and human monocyte cells, the organic compounds and the aging of the aerosol were major drivers of the cell level toxicity of aerosol (Hakkarainen et al., 2022).

In this work, we found that the majority of low-volatility condensable vapors in Helsinki were impacted by both biogenic and anthropogenic precursors, despite high local anthropogenic emissions. The VOC precursors themselves were mostly of biogenic origin, i.e. BVOC, but the oxidation process was strongly perturbed by anthropogenic activity, particularly by NO_x. While detailed similarities in mass spectra of factors were often small between the close-by sites studied here, most observed compounds at both stations were ONCs. Previous studies have shown that NO_x can change the yield of SOA formation during VOC oxidation (Mutzel et al., 2021; Jaoui et al., 2013; Ng et al., 2017), though this effect may be not as clear to observe in ambient measurements (Yan et al., 2022). In the smaller m/Q ranges studied in this work, the influence from AVOC was larger, but we cannot deduce the impact of these factors on SOA formation due to their semi-volatile nature. Nevertheless, our results indicate that in Helsinki, and likely in other biologically influenced urban areas, anthropogenic emissions affect HOM formation and composition most strongly by the participation of NO_x in the (B)VOC

555 oxidation. That influence will be propagated to the SOA, both concerning the composition as well as the effective yield
556 of SOA from the BVOC oxidation, but quantifying the ultimate impact on either of these will require further studies.

557 4. Conclusions

558 We measured the composition of condensable vapors, HOM, during late spring at two stations separated by 900 m in
559 different sub-environments in Helsinki, a city with considerable biogenic influence from trees. We compared HOM
560 composition and formation pathways at the two sites, an urban background station and a street canyon, using PMF analysis
561 to separate the complex data into covarying compound groups. We found that the majority of the HOM originated from
562 BVOCs at both locations, despite them being dominated by AVOC emissions (Rantala et al., 2016; Saarikoski et al.,
563 2023). However, we did observe a strong anthropogenic influence on the HOM formation, due to the elevated NO_x
564 concentrations at both stations, which is consistent with previous studies conducted in urban environments (Guo et al.,
565 2022b; Liu et al., 2021; Nie et al., 2022). The PMF factors, and their temporal behavior, were surprisingly different
566 between the two sites, considering their relatively close proximity. Monoterpene-derived dimers were the compound
567 groups that correlated best between the sites. On the contrary, at the street canyon site we observed a factor corresponding
568 partly to AVOC-derived factors found in Chinese megacities (Guo et al., 2022b; Liu et al., 2021; Nie et al., 2022). The
569 lack of a similar factor in the PMF solution from the urban background station highlights that HOM composition at two
570 nearby sites in an urban environment can differ noticeably depending on the local anthropogenic influences. To a large
571 extent, we expect this difference to be driven by differences in the environmental conditions, leading to distinct oxidation
572 products even when the same VOC molecule becomes oxidized, due to competition between both oxidants and RO₂
573 terminators.

574 Our work indicates that when analyzing and discussing the impact of HOM on SOA and air quality in urban environments,
575 we need to keep in mind the spatial inhomogeneity of urban areas in the HOM composition and formation mechanisms.
576 Thus, a more detailed investigation of the formation and composition of HOM in a variety of different urban sub-
577 environments would be beneficial. Additionally, our findings are restricted to a short and biologically active period, hence
578 follow-up research on seasonal changes is needed. Finally, we recommend that future mass spectrometric studies in urban
579 area employ devices with resolving power above 5000 Th/Th, as the mass spectra are extremely complex and thus even
580 peak identification can be a major challenge.

581 Data availability

582 PMF factors and VOC data used for this study are available at <https://doi.org/10.5281/zenodo.8273030> (Okuljar et al.,
583 2023). SA, sub-3 nm particle concentration as well as meteorological and trace gas data from street canyon are available
584 at <https://doi.org/10.5281/zenodo.4884875> (Okuljar, 2021). Trace gas and meteorological data measured at the
585 background station are available at the SmartSMEAR data repository (<https://avaa.tdata.fi/web/smart>, last access: 22
586 August 2023; Junninen et al., 2009).

587 Author contribution

588 The main ideas were formulated by OG, HT, JKo, JVM, MS, MDM TR, TP, MK and the results were interpreted by
589 MOk, OG, PP, and ME. TR, HK, OG, HT prepared measurement methodology and OG, MOI, JKa, HH, and HK
590 contributed to data collection. MOk performed the data analysis and YZ supported it. OG and ME supervised the project.

591 HT, MDM, and TP made a funding acquisition. MOK visualized data and prepared the manuscript with contributions
592 from OG, ME. All the authors reviewed and commented the manuscript.

593 Competing interests

594 The authors declare that they have no conflict of interest.

595 Acknowledgments.

596 This research was supported by the Regional innovations and experimentations funds AIKO (project HAQT, AIKO014),
597 Business Finland (CITYZER project, Tekes nro: 3021/31/2015 and 2883/31/2015), Pegasor Oy and HSY, Academy of
598 Finland (grant nos 273010, 307331, 310626, 311932, 318940, 1325656, 326437, and ACCC flagship grant no. 337549,
599 337552, 337551), Healthy Outdoor Premises for Everyone (HOPE), Urban Innovation Actions, Regional development
600 funds, The Technology Industries of Finland Centennial Foundation via project Urbaani ilmanlaatu 2.0, European
601 Commission via Horizon Europe project “Non-CO2 Forcers and their Climate, Weather, Air Quality and Health Impacts,
602 FOCI” (101056783), Faculty of Science 3-year grant (75284132), Tampere University of Technology graduate school,
603 European Research Council (ERC) project ADAPT (grant no. 101002728), European Union Horizon 2020 research and
604 innovation programme (grant no 101036245, RI-URBANS; grant no. 821205, FORCeS, and ERA-PLANET project
605 SMURBS, 689443).

606 We would like to thank the people who took care of instruments and helped with measurements at the SMEAR III (Pekka
607 Rantala, Erkki Siivola, Pasi Aalto, Petri Keronen, Frans Korhonen, Tiia Laurila, Lauriane Quéléver, Tuuli Lehmusjärvi,
608 Deniz Kemppainen) and the HSY Mäkelänkatu site (Anssi Julkunen, Anders Svens, Harri Portin, Taneli Mäkelä, Tommi
609 Wallenius, Anu Kousa).

610 References

611 Anderson, J. O., Thundiyil, J. G., and Stolbach, A.: Clearing the Air: A Review of the Effects of Particulate Matter Air
612 Pollution on Human Health, *J. Med. Toxicol.*, 8, 166–175, <https://doi.org/10.1007/s13181-011-0203-1>, 2012.

613 Atkinson, R. and Arey, J.: Atmospheric degradation of volatile organic compounds, *Chem. Rev.*, 103, 4605–4638,
614 <https://doi.org/10.1021/CR0206420>, 2003.

615 Bianchi, F., Garmash, O., He, X., Yan, C., Iyer, S., Rosendahl, I., Xu, Z., Rissanen, M. P., Riva, M., Taipale, R.,
616 Sarnela, N., Petäjä, T., Worsnop, D. R., Kulmala, M., Ehn, M., and Junninen, H.: The role of highly oxygenated
617 molecules (HOMs) in determining the composition of ambient ions in the boreal forest, *Atmos. Chem. Phys.*, 17,
618 13819–13831, <https://doi.org/10.5194/ACP-17-13819-2017>, 2017.

619 Bianchi, F., Kurtén, T., Riva, M., Mohr, C., Rissanen, M. P., Roldin, P., Berndt, T., Crounse, J. D., Wennberg, P. O.,
620 Mentel, T. F., Wildt, J., Junninen, H., Jokinen, T., Kulmala, M., Worsnop, D. R., Thornton, J. A., Donahue, N.,
621 Kjaergaard, H. G., and Ehn, M.: Highly Oxygenated Organic Molecules (HOM) from Gas-Phase Autoxidation
622 Involving Peroxy Radicals: A Key Contributor to Atmospheric Aerosol, *Chem. Rev.*, 119, 3472–3509,
623 <https://doi.org/10.1021/ACS.CHEMREV.8B00395>, 2019.

624 Brean, J., Harrison, R. M., Shi, Z., Beddows, D. C. S., Acton, W. J. F., Nicholas Hewitt, C., Squires, F. A., and Lee, J.:
625 Observations of highly oxidized molecules and particle nucleation in the atmosphere of Beijing, *Atmos. Chem. Phys.*,

19, 14933–14947, <https://doi.org/10.5194/ACP-19-14933-2019>, 2019.

Burnett, R. T., Arden Pope, C., Ezzati, M., Olives, C., Lim, S. S., Mehta, S., Shin, H. H., Singh, G., Hubbell, B., Brauer, M., Ross Anderson, H., Smith, K. R., Balmes, J. R., Bruce, N. G., Kan, H., Laden, F., Prüss-Ustün, A., Turner, M. C., Gapstur, S. M., Diver, W. R., and Cohen, A.: An Integrated Risk Function for Estimating the Global Burden of Disease Attributable to Ambient Fine Particulate Matter Exposure, *Environ. Health Perspect.*, 122, 397–403, <https://doi.org/10.1289/EHP.1307049>, 2014.

Canonaco, F., Crippa, M., Slowik, J. G., Baltensperger, U., and Prévôt, A. S. H.: SoFi, an IGOR-based interface for the efficient use of the generalized multilinear engine (ME-2) for the source apportionment: ME-2 application to aerosol mass spectrometer data, *Atmos. Meas. Tech.*, 6, 3649–3661, <https://doi.org/10.5194/AMT-6-3649-2013>, 2013.

Chen, G., Canonaco, F., Tobler, A., Aas, W., Alastuey, A., Allan, J., Atabakhsh, S., Aurela, M., Baltensperger, U., Bougiatioti, A., De Brito, J. F., Ceburnis, D., Chazeau, B., Chebaicheb, H., Daellenbach, K. R., Ehn, M., El Haddad, I., Eleftheriadis, K., Favez, O., Flentje, H., Font, A., Fossum, K., Freney, E., Gini, M., Green, D. C., Heikkinen, L., Herrmann, H., Kalogridis, A. C., Keernik, H., Lhotka, R., Lin, C., Lunder, C., Maasikmets, M., Manousakas, M. I., Marchand, N., Marin, C., Marmureanu, L., Mihalopoulos, N., Močnik, G., Nęcki, J., O’Dowd, C., Ovadnevaite, J., Peter, T., Petit, J. E., Pikridas, M., Matthew Platt, S., Pokorná, P., Poulain, L., Priestman, M., Riffault, V., Rinaldi, M., Rózański, K., Schwarz, J., Sciare, J., Simon, L., Skiba, A., Slowik, J. G., Sosedova, Y., Stavroulas, I., Styszko, K., Teinmaa, E., Timonen, H., Tremper, A., Vasilescu, J., Via, M., Vodička, P., Wiedensohler, A., Zografou, O., Cruz Minguillón, M., and Prévôt, A. S. H.: European aerosol phenomenology – 8: Harmonised source apportionment of organic aerosol using 22 Year-long ACSM/AMS datasets, *Environ. Int.*, 166, 107325, <https://doi.org/10.1016/J.ENVINT.2022.107325>, 2022.

Coggon, M. M., Gkatzelis, G. I., McDonald, B. C., Gilman, J. B., Schwantes, R. H., Abuhassan, N., Aikin, K. C., Arendt, M. F., Berkoff, T. A., Brown, S. S., Campos, T. L., Dickerson, R. R., Gronoff, G., Hurley, J. F., Isaacman-Vanwertz, G., Koss, A. R., Li, M., McKeen, S. A., Moshary, F., Peischl, J., Pospisilova, V., Ren, X., Wilson, A., Wu, Y., Trainer, M., and Warneke, C.: Volatile chemical product emissions enhance ozone and modulate urban chemistry, *Proc. Natl. Acad. Sci. U. S. A.*, 118, e2026653118, <https://doi.org/10.1073/pnas.2026653118>, 2021.

Cohen, A. J., Brauer, M., Burnett, R., Anderson, H. R., Frostad, J., Estep, K., Balakrishnan, K., Brunekreef, B., Dandona, L., Dandona, R., Feigin, V., Freedman, G., Hubbell, B., Jobling, A., Kan, H., Knibbs, L., Liu, Y., Martin, R., Morawska, L., Pope, C. A., Shin, H., Straif, K., Shaddick, G., Thomas, M., van Dingenen, R., van Donkelaar, A., Vos, T., Murray, C. J. L., and Forouzanfar, M. H.: Estimates and 25-year trends of the global burden of disease attributable to ambient air pollution: an analysis of data from the Global Burden of Diseases Study 2015, *Lancet*, 389, 1907–1918, [https://doi.org/10.1016/S0140-6736\(17\)30505-6](https://doi.org/10.1016/S0140-6736(17)30505-6), 2017.

Crounse, J. D., Nielsen, L. B., Jørgensen, S., Kjaergaard, H. G., and Wennberg, P. O.: Autoxidation of organic compounds in the atmosphere, *J. Phys. Chem. Lett.*, 4, 3513–3520, <https://doi.org/10.1021/jz4019207>, 2013.

Crutzen, P. J., Lawrence, M. G., and Pöschl, U.: On the background photochemistry of tropospheric ozone, *Tellus, Ser. B Chem. Phys. Meteorol.*, 51, 123–146, <https://doi.org/10.1034/J.1600-0889.1999.00010.X>, 1999.

Dam, M., Draper, D. C., Marsavin, A., Fry, J. L., and Smith, J. N.: Observations of gas-phase products from the nitrate-radical-initiated oxidation of four monoterpenes, *Atmos. Chem. Phys.*, 22, 9017–9031, <https://doi.org/10.5194/ACP-22->

9017-2022, 2022.

Ehn, M., Thornton, J. A., Kleist, E., Sipilä, M., Junninen, H., Pullinen, I., Springer, M., Rubach, F., Tillmann, R., Lee, B., Lopez-Hilfiker, F., Andres, S., Acir, I. H., Rissanen, M., Jokinen, T., Schobesberger, S., Kangasluoma, J., Kontkanen, J., Nieminen, T., Kurtén, T., Nielsen, L. B., Jørgensen, S., Kjaergaard, H. G., Canagaratna, M., Maso, M. D., Berndt, T., Petäjä, T., Wahner, A., Kerminen, V. M., Kulmala, M., Worsnop, D. R., Wildt, J., and Mentel, T. F.: A large source of low-volatility secondary organic aerosol, *Nature*, 506, 476–479, <https://doi.org/10.1038/nature13032>, 2014.

Fry, J. L., Draper, D. C., Barsanti, K. C., Smith, J. N., Ortega, J., Winkler, P. M., Lawler, M. J., Brown, S. S., Edwards, P. M., Cohen, R. C., and Lee, L.: Secondary organic aerosol formation and organic nitrate yield from NO₃ oxidation of biogenic hydrocarbons, *Environ. Sci. Technol.*, 48, 11944–11953, <https://doi.org/10.1021/es502204x>, 2014.

Garmash, O., Rissanen, M. P., Pullinen, I., Schmitt, S., Kausiala, O., Tillmann, R., Zhao, D., Percival, C., Bannan, T. J., Priestley, M., Hallquist, Å. M., Kleist, E., Kiendler-Scharr, A., Hallquist, M., Berndt, T., McFiggans, G., Wildt, J. J., Mentel, T. F., Ehn, M., Hallquist, A. M., Kleist, E., Kiendler-Scharr, A., Hallquist, M., Berndt, T., McFiggans, G., Wildt, J. J., Mentel, T. F., and Ehn, M.: Multi-generation OH oxidation as a source for highly oxygenated organic molecules from aromatics, *Atmos. Chem. Phys.*, 20, 515–537, <https://doi.org/10.5194/acp-20-515-2020>, 2020.

Gkatzelis, G. I., Coggon, M. M., McDonald, B. C., Peischl, J., Gilman, J. B., Aikin, K. C., Robinson, M. A., Canonaco, F., Prevot, A. S. H., Trainer, M., and Warneke, C.: Observations Confirm that Volatile Chemical Products Are a Major Source of Petrochemical Emissions in U.S. Cities, *Environ. Sci. Technol.*, 55, 4332–4343, <https://doi.org/10.1021/acs.est.0c05471>, 2021.

Guo, Y., Shen, H., Pullinen, I., Luo, H., Kang, S., Vereecken, L., Fuchs, H., Hallquist, M., Acir, I. H., Tillmann, R., Rohrer, F., Wildt, J., Kiendler-Scharr, A., Wahner, A., Zhao, D., and Mentel, T. F.: Identification of highly oxygenated organic molecules and their role in aerosol formation in the reaction of limonene with nitrate radical, *Atmos. Chem. Phys.*, 22, 11323–11346, <https://doi.org/10.5194/ACP-22-11323-2022>, 2022a.

Guo, Y., Yan, C., Liu, Y., Qiao, X., Zheng, F., Zhang, Y., Zhou, Y., Li, C., Fan, X., Lin, Z., Feng, Z., Zhang, Y., Zheng, P., Tian, L., Nie, W., Wang, Z., Huang, D., Daellenbach, K. R., Yao, L., Dada, L., Bianchi, F., Jiang, J., Liu, Y., Kerminen, V. M., and Kulmala, M.: Seasonal variation in oxygenated organic molecules in urban Beijing and their contribution to secondary organic aerosol, *Atmos. Chem. Phys.*, 22, 10077–10097, <https://doi.org/10.5194/ACP-22-10077-2022>, 2022b.

Hakkarainen, H., Salo, L., Mikkonen, S., Saarikoski, S., Aurela, M., Teinilä, K., Ihalainen, M., Martikainen, S., Marjanen, P., Lepistö, T., Kuittinen, N., Saarnio, K., Aakko-Saksa, P., Pfeiffer, T. V., Timonen, H., Rönkkö, T., and Jalava, P. I.: Black carbon toxicity dependence on particle coating: Measurements with a novel cell exposure method, *Sci. Total Environ.*, 838, 156543, <https://doi.org/10.1016/J.SCITOTENV.2022.156543>, 2022.

Helin, A., Hakola, H., and Hellén, H.: Optimisation of a thermal desorption-gas chromatography-mass spectrometry method for the analysis of monoterpenes, sesquiterpenes and diterpenes, *Atmos. Meas. Tech.*, 13, 3543–3560, <https://doi.org/10.5194/AMT-13-3543-2020>, 2020.

Hyttinen, N., Kupiainen-Määttä, O., Rissanen, M. P., Muuronen, M., Ehn, M., and Kurtén, T.: Modeling the Charging

699 of Highly Oxidized Cyclohexene Ozonolysis Products Using Nitrate-Based Chemical Ionization, *J. Phys. Chem. A*,
700 119, 6339–6345, <https://doi.org/10.1021/acs.jpca.5b01818>, 2015.

701 Jaoui, M., Kleindienst, T. E., Docherty, K. S., Lewandowski, M., Offenberg, J. H., Jaoui, M., Kleindienst, T. E.,
702 Docherty, K. S., Lewandowski, M., and Offenberg, J. H.: Secondary organic aerosol formation from the oxidation of a
703 series of sesquiterpenes: α -cedrene, β -caryophyllene, α -humulene and α -farnesene with O₃, OH and NO₃ radicals,
704 *Environ. Chem.*, 10, 178–193, <https://doi.org/10.1071/EN13025>, 2013.

705 Järvi, L., Hannuniemi, H., Hussein, T., Junninen, H., Aalto, P. P., Hillamo, R., Mäkelä, T., Keronen, P., Siivola, E.,
706 Vesala, T., and Kulmala, M.: The urban measurement station SMEAR III: Continuous monitoring of air pollution and
707 surface-atmosphere interactions in Helsinki, Finland, *Boreal Environ. Res.*, 14, 86–109, 2009.

708 Järvi, L., Kurppa, M., Kuuluvainen, H., Rönkkö, T., Karttunen, S., Balling, A., Timonen, H., Niemi, J. V., and Pirjola,
709 L.: Determinants of spatial variability of air pollutant concentrations in a street canyon network measured using a
710 mobile laboratory and a drone, *Sci. Total Environ.*, 856, 158974, <https://doi.org/10.1016/J.SCITOTENV.2022.158974>,
711 2023.

712 Jokinen, T., Sipilä, M., Junninen, H., Ehn, M., Lönn, G., Hakala, J., Petäjä, T., Mauldin, R. L., Kulmala, M., Worsnop,
713 D. R., Mauldin III, R. L., Kulmala, M., and Worsnop, D. R.: Atmospheric sulphuric acid and neutral cluster
714 measurements using CI-API-TOF, *Atmos. Chem. Phys.*, 12, 4117–4125, <https://doi.org/10.5194/acp-12-4117-2012>,
715 2012.

716 Junninen, H., Lauri, A., Keronen, P., Aalto, P., Hiltunen, V., Hari, P., and Kulmala, M.: Smart-SMEAR: on-line data
717 exploration and visualization tool for SMEAR stations, *Boreal Environ. Res.*, 14, 447–457, 2009.

718 Junninen, H., Ehn, M., Petäjä, T., Luosujärvi, L., Kotiaho, T., Kostianen, R., Rohner, U., Gonin, M., Fuhrer, K.,
719 Kulmala, M., and Worsnop, D. R.: A high-resolution mass spectrometer to measure atmospheric ion composition,
720 *Atmos. Meas. Tech.*, 3, 1039–1053, <https://doi.org/10.5194/amt-3-1039-2010>, 2010.

721 Kaltsonoudis, C., Kostenidou, E., Florou, K., Psichoudaki, M., and Pandis, S. N.: Temporal variability and sources of
722 VOCs in urban areas of the eastern Mediterranean, *Atmos. Chem. Phys.*, 16, 14825–14842, [https://doi.org/10.5194/acp-](https://doi.org/10.5194/acp-16-14825-2016)
723 16-14825-2016, 2016.

724 Karl, T., Striednig, M., Graus, M., Hammerle, A., and Wohlfahrt, G.: Urban flux measurements reveal a large pool of
725 oxygenated volatile organic compound emissions, *Proc. Natl. Acad. Sci. U. S. A.*, 115, 1186–1191, [https://doi.org/](https://doi.org/10.1073/pnas.1714715115)
726 10.1073/pnas.1714715115, 2018.

727 Kaser, L., Peron, A., Graus, M., Striednig, M., Wohlfahrt, G., Juran, S., and Karl, T.: Interannual variability of
728 terpenoid emissions in an alpine city, *Atmos. Chem. Phys.*, 22, 5603–5618, <https://doi.org/10.5194/ACP-22-5603-2022>,
729 2022.

730 Kota, S. H., Park, C., Hale, M. C., Werner, N. D., Schade, G. W., and Ying, Q.: Estimation of VOC emission factors
731 from flux measurements using a receptor model and footprint analysis, *Atmos. Environ.*, 82, 24–35,
732 <https://doi.org/10.1016/J.ATMOSENV.2013.09.052>, 2014.

733 Kroll, J. H. and Seinfeld, J. H.: Chemistry of secondary organic aerosol: Formation and evolution of low-volatility

734 organics in the atmosphere, *Atmos. Environ.*, 42, 3593–3624, <https://doi.org/10.1016/J.ATMOSENV.2008.01.003>,
735 2008.

736 Kürten, A., Bergen, A., Heinritzi, M., Leiminger, M., Lorenz, V., Piel, F., Simon, M., Sitals, R., Wagner, A. C., and
737 Curtius, J.: Observation of new particle formation and measurement of sulfuric acid, ammonia, amines and highly
738 oxidized organic molecules at a rural site in central Germany, *Atmos. Chem. Phys.*, 16, 12793–12813,
739 <https://doi.org/10.5194/acp-16-12793-2016>, 2016.

740 Kuuluvainen, H., Poikkimäki, M., Järvinen, A., Kuula, J., Irijala, M., Dal Maso, M., Keskinen, J., Timonen, H., Niemi,
741 J. V., and Rönkkö, T.: Vertical profiles of lung deposited surface area concentration of particulate matter measured with
742 a drone in a street canyon, *Environ. Pollut.*, 241, 96–105, <https://doi.org/10.1016/j.envpol.2018.04.100>, 2018.

743 Li, X.-B., Yuan, B., Wang, S., Wang, C., Lan, J., Liu, Z., Song, Y., He, X., Huangfu, Y., Pei, C., Cheng, P., Yang, S.,
744 Qi, J., Wu, C., Huang, S., You, Y., Chang, M., Zheng, H., Yang, W., Wang, X., and Shao, M.: Variations and sources
745 of volatile organic compounds (VOCs) in urban region: insights from measurements on a tall tower, *Atmos. Chem.*
746 *Phys.*, 22, 10567–10587, <https://doi.org/10.5194/acp-22-10567-2022>, 2022.

747 Lim, S. S., Vos, T., Flaxman, A. D., Danaei, G., Shibuya, K., Adair-Rohani, H., Amann, M., Anderson, H. R., Andrews,
748 K. G., Aryee, M., Atkinson, C., Bacchus, L. J., Bahalim, A. N., Balakrishnan, K., Balmes, J., Barker-Collo, S., Baxter,
749 A., Bell, M. L., Blore, J. D., Blyth, F., Bonner, C., Borges, G., Bourne, R., Boussinesq, M., Brauer, M., Brooks, P.,
750 Bruce, N. G., Brunekreef, B., Bryan-Hancock, C., Bucello, C., Buchbinder, R., Bull, F., Burnett, R. T., Byers, T. E.,
751 Calabria, B., Carapetis, J., Carnahan, E., Chafe, Z., Charlson, F., Chen, H., Chen, J. S., Cheng, A. T. A., Child, J. C.,
752 Cohen, A., Colson, K. E., Cowie, B. C., Darby, S., Darling, S., Davis, A., Degenhardt, L., Dentener, F., Des Jarlais, D.
753 C., Devries, K., Dherani, M., Ding, E. L., Dorsey, E. R., Driscoll, T., Edmond, K., Ali, S. E., Engell, R. E., Erwin, P. J.,
754 Fahimi, S., Falder, G., Farzadfar, F., Ferrari, A., Finucane, M. M., Flaxman, S., Fowkes, F. G. R., Freedman, G.,
755 Freeman, M. K., Gakidou, E., Ghosh, S., Giovannucci, E., Gmel, G., Graham, K., Grainger, R., Grant, B., Gunnell, D.,
756 Gutierrez, H. R., Hall, W., Hoek, H. W., Hogan, A., Hosgood, H. D., Hoy, D., Hu, H., Hubbell, B. J., Hutchings, S. J.,
757 Ibeanusi, S. E., Jacklyn, G. L., Jasrasaria, R., Jonas, J. B., Kan, H., Kanis, J. A., Kassebaum, N., Kawakami, N., Khang,
758 Y. H., Khatibzadeh, S., Khoo, J. P., Kok, C., et al.: A comparative risk assessment of burden of disease and injury
759 attributable to 67 risk factors and risk factor clusters in 21 regions, 1990–2010: A systematic analysis for the Global
760 Burden of Disease Study 2010, *Lancet*, 380, 2224–2260, [https://doi.org/10.1016/S0140-6736\(12\)61766-8](https://doi.org/10.1016/S0140-6736(12)61766-8), 2012.

761 Liu, S. C., Kley, D., McFarland, M., Mahlman, J. D., and Levy, H.: On the origin of tropospheric ozone., *J. Geophys.*
762 *Res.*, 85, 7546–7552, <https://doi.org/10.1029/JC085IC12P07546>, 1980.

763 Liu, Y., Nie, W., Li, Y., Ge, D., Liu, C., Xu, Z., Chen, L., Wang, T., Wang, L., Sun, P., Qi, X., Wang, J., Xu, Z., Yuan,
764 J., Yan, C., Zhang, Y., Huang, D., Wang, Z., Donahue, N. M., Worsnop, D., Chi, X., Ehn, M., and Dİng, A.: Formation
765 of condensable organic vapors from anthropogenic and biogenic volatile organic compounds (VOCs) is strongly
766 perturbed by NO_x in eastern China, *Atmos. Chem. Phys.*, 21, 14789–14814, [https://doi.org/10.5194/ACP-21-14789-](https://doi.org/10.5194/ACP-21-14789-2021)
767 2021, 2021.

768 Massoli, P., Stark, H., Canagaratna, M. R., Krechmer, J. E., Xu, L., Ng, N. L., Mauldin, R. L., Yan, C., Kimmel, J.,
769 Misztal, P. K., Jimenez, J. L., Jayne, J. T., and Worsnop, D. R.: Ambient Measurements of Highly Oxidized Gas-Phase
770 Molecules during the Southern Oxidant and Aerosol Study (SOAS) 2013, *ACS Earth Sp. Chem.*, 2, 653–672,

771 <https://doi.org/10.1021/acsearthspacechem.8b00028>, 2018.

772 McDonald, B. C., De Gouw, J. A., Gilman, J. B., Jathar, S. H., Akherati, A., Cappa, C. D., Jimenez, J. L., Lee-Taylor,
 773 J., Hayes, P. L., McKeen, S. A., Cui, Y. Y., Kim, S. W., Gentner, D. R., Isaacman-VanWertz, G., Goldstein, A. H.,
 774 Harley, R. A., Frost, G. J., Roberts, J. M., Ryerson, T. B., and Trainer, M.: Volatile chemical products emerging as
 775 largest petrochemical source of urban organic emissions, *Science* (80-.), 359, 760–764,
 776 <https://doi.org/10.1126/science.aag0524>, 2018.

777 Molteni, U., Bianchi, F., Klein, F., El Haddad, I., Frege, C., Rossi, M. J., Dommen, J., and Baltensperger, U.: Formation
 778 of highly oxygenated organic molecules from aromatic compounds, *Atmos. Chem. Phys.*, 18, 1909–1921,
 779 <https://doi.org/10.5194/acp-18-1909-2018>, 2018.

780 Mutzel, A., Zhang, Y., Böge, O., Rodigast, M., Kolodziejczyk, A., Wang, X., and Herrmann, H.: Importance of
 781 secondary organic aerosol formation of α / i -pinene, limonene, and m / i -cresol comparing day- And nighttime radical
 782 chemistry, *Atmos. Chem. Phys.*, 21, 8479–8498, <https://doi.org/10.5194/ACP-21-8479-2021>, 2021.

783 Ng, N. L., Herndon, S. C., Trimborn, A., Canagaratna, M. R., Croteau, P. L., Onasch, T. B., Sueper, D., Worsnop, D.
 784 R., Zhang, Q., Sun, Y. L., and Jayne, J. T.: An Aerosol Chemical Speciation Monitor (ACSM) for Routine Monitoring
 785 of the Composition and Mass Concentrations of Ambient Aerosol, 45, 780–794,
 786 <https://doi.org/10.1080/02786826.2011.560211>, 2011.

787 Ng, N. L., Brown, S. S., Archibald, A. T., Atlas, E., Cohen, R. C., Crowley, J. N., Day, D. A., Donahue, N. M., Fry, J.
 788 L., Fuchs, H., Griffin, R. J., Guzman, M. I., Herrmann, H., Hodzic, A., Iinuma, Y., Jimenez, J. L., Kiendler-Scharr, A.,
 789 Lee, B. H., Luecken, D. J., Mao, J., McLaren, R., Mutzel, A., Osthoff, H. D., Picquet-Varrau, B., Platt, U., Pye, H. O.
 790 T., Rudich, Y., Schwantes, R. H., Shiraiwa, M., Stutz, J., Thornton, J. A., Tilgner, A., Williams, B. J., and Zaveri, R.
 791 A.: Nitrate radicals and biogenic volatile organic compounds: oxidation, mechanisms, and organic aerosol, *Atmos.*
 792 *Chem. Phys.*, 17, 2103–2162, <https://doi.org/10.5194/acp-17-2103-2017>, 2017.

793 Nie, W., Yan, C., Huang, D. D., Wang, Z., Liu, Y., Qiao, X., Guo, Y., Tian, L., Zheng, P., Xu, Z., Li, Y., Xu, Z., Qi, X.,
 794 Sun, P., Wang, J., Zheng, F., Li, X., Yin, R., Dallenbach, K. R., Bianchi, F., Petäjä, T., Zhang, Y., Wang, M., Schervish,
 795 M., Wang, S., Qiao, L., Wang, Q., Zhou, M., Wang, H., Yu, C., Yao, D., Guo, H., Ye, P., Lee, S., Li, Y. J., Liu, Y., Chi,
 796 X., Kerminen, V.-M., Ehn, M., Donahue, N. M., Wang, T., Huang, C., Kulmala, M., Worsnop, D., Jiang, J., and Ding,
 797 A.: Secondary organic aerosol formed by condensing anthropogenic vapours over China’s megacities, *Nat. Geosci.*
 798 2022, 1–7, <https://doi.org/10.1038/s41561-022-00922-5>, 2022.

799 Nie, W., Yan, C., Yang, L., Roldin, P., Liu, Y., Vogel, A. L., Molteni, U., Stolzenburg, D., Finkenzeller, H., Amorim,
 800 A., Bianchi, F., Curtius, J., Dada, L., Draper, D. C., Duplissy, J., Hansel, A., He, X. C., Hofbauer, V., Jokinen, T., Kim,
 801 C., Lehtipalo, K., Nie, L., Mauldin, R. L., Makhmutov, V., Mentler, B., Mizelli-Ojdanic, A., Petäjä, T., Quéléver,
 802 L. L. J., Schallhart, S., Simon, M., Tauber, C., Tomé, A., Volkamer, R., Wagner, A. C., Wagner, R., Wang, M., Ye, P.,
 803 Li, H., Huang, W., Qi, X., Lou, S., Liu, T., Chi, X., Dommen, J., Baltensperger, U., El Haddad, I., Kirkby, J., Worsnop,
 804 D., Kulmala, M., Donahue, N. M., Ehn, M., and Ding, A.: NO at low concentration can enhance the formation of highly
 805 oxygenated biogenic molecules in the atmosphere, *Nat. Commun.* 2023 141, 14, 1–11, [https://doi.org/10.1038/s41467-](https://doi.org/10.1038/s41467-023-39066-4)
 806 023-39066-4, 2023.

807 Okuljar, M.: Measurement report: The influence of traffic and new particle formation on the size distribution of 1–800

808 nm particles in Helsinki: a street canyon and an urban background station comparison [Data set],
 809 <https://doi.org/10.5281/zenodo.4884875>, 2021.

810 Okuljar, M., Kuuluvainen, H., Kontkanen, J., Garmash, O., Olin, M., Niemi, J. V., Timonen, H., Kangasluoma, J.,
 811 Tham, Y. J., Baalbaki, R., Sipilä, M., Salo, L., Lintusaari, H., Portin, H., Teinilä, K., Aurela, M., Dal Maso, M.,
 812 Rönkkö, T., Petäjä, T., and Paasonen, P.: Measurement report: The influence of traffic and new particle formation on
 813 the size distribution of 1-800nm particles in Helsinki-a street canyon and an urban background station comparison,
 814 *Atmos. Chem. Phys.*, 21, 9931–9953, <https://doi.org/10.5194/ACP-21-9931-2021>, 2021.

815 Okuljar, M., Garmash, O., Olin, M., Kalliokoski, J., Timonen, H., Niemi, J. V., Paasonen, P., Kontkanen, J., Zhang, Y.,
 816 Hellén, H., Kuuluvainen, H., Aurela, M., Manninen, H. E., Sipilä, M., Rönkkö, T., Petäjä, T., Kulmala, M., Dal Maso,
 817 M., and Ehn, M.: Dataset from “Influence of anthropogenic emissions on the composition of highly oxygenated organic
 818 molecules in Helsinki: a street canyon and urban background station comparison” [Data set],
 819 <https://doi.org/10.5281/zenodo.8273030>, 2023.

820 Olin, M., Kuuluvainen, H., Aurela, M., Kalliokoski, J., Kuittinen, N., Isotalo, M., Timonen, H. J., Niemi, J. V., Rönkkö,
 821 T., and Dal Maso, M.: Traffic-originated nanocluster emission exceeds H₂SO₄-driven photochemical new particle
 822 formation in an urban area, *Atmos. Chem. Phys.*, 20, 1–13, <https://doi.org/10.5194/acp-20-1-2020>, 2020.

823 Paatero, P.: Least squares formulation of robust non-negative factor analysis, *Chemom. Intell. Lab. Syst.*, 37, 23–35,
 824 [https://doi.org/10.1016/S0169-7439\(96\)00044-5](https://doi.org/10.1016/S0169-7439(96)00044-5), 1997.

825 Paatero, P.: The Multilinear Engine—A Table-Driven, Least Squares Program for Solving Multilinear Problems,
 826 Including the n-Way Parallel Factor Analysis Model, 8, 854–888, <https://doi.org/10.1080/10618600.1999.10474853>,
 827 1999.

828 Paatero, P. and Hopke, P. K.: Discarding or downweighting high-noise variables in factor analytic models, *Anal. Chim.*
 829 *Acta*, 490, 277–289, [https://doi.org/10.1016/S0003-2670\(02\)01643-4](https://doi.org/10.1016/S0003-2670(02)01643-4), 2003.

830 Paatero, P. and Tapper, U.: Positive matrix factorization: A non-negative factor model with optimal utilization of error
 831 estimates of data values, *Environmetrics*, 5, 111–126, <https://doi.org/10.1002/ENV.3170050203>, 1994.

832 Pandis, S. N., Harley, R. A., Cass, G. R., and Seinfeld, J. H.: Secondary organic aerosol formation and transport,
 833 *Atmos. Environ. Part A, Gen. Top.*, 26, 2269–2282, [https://doi.org/10.1016/0960-1686\(92\)90358-R](https://doi.org/10.1016/0960-1686(92)90358-R), 1992.

834 Peräkylä, O., Riva, M., Heikkinen, L., Quéléver, L., Roldin, P., and Ehn, M.: Experimental investigation into the
 835 volatilities of highly oxygenated organic molecules (HOMs), *Atmos. Chem. Phys.*, 20, 649–669,
 836 <https://doi.org/10.5194/acp-20-649-2020>, 2020.

837 Pope, C. A. and Dockery, D. W.: Health Effects of Fine Particulate Air Pollution: Lines that Connect, 56, 709–742,
 838 <https://doi.org/10.1080/10473289.2006.10464485>, 2012.

839 Pullinen, I., Schmitt, S., Kang, S., Sarrafzadeh, M., Schlag, P., Andres, S., Kleist, E., Mentel, T. F., Rohrer, F.,
 840 Springer, M., Tillmann, R., Wildt, J., Wu, C., Zhao, D., Wahner, A., and Kiendler-Scharr, A.: Impact of NO_x on
 841 secondary organic aerosol (SOA) formation from α -pinene and β -pinene photooxidation: The role of highly oxygenated
 842 organic nitrates, *Atmos. Chem. Phys.*, 20, 10125–10147, <https://doi.org/10.5194/ACP-20-10125-2020>, 2020.

843 Quelever, L. L. J., Kristensen, K., Normann Jensen, L., Rosati, B., Teiwes, R., Daellenbach, K. R., Peräkylä, O., Roldin,
 844 P., Bossi, R., Pedersen, H. B., Glasius, M., Bilde, M., and Ehn, M.: Effect of temperature on the formation of highly
 845 oxygenated organic molecules (HOMs) from alpha-pinene ozonolysis, *Atmos. Chem. Phys.*, 19, 7609–7625,
 846 <https://doi.org/10.5194/ACP-19-7609-2019>, 2019.

847 Rantala, P., Järvi, L., Taipale, R., Laurila, T. K., Patokoski, J., Kajos, M. K., Kurppa, M., Haapanala, S., Siivola, E.,
 848 Petäjä, T., Ruuskanen, T. M., and Rinne, J.: Anthropogenic and biogenic influence on VOC fluxes at an urban
 849 background site in Helsinki, Finland, *Atmos. Chem. Phys.*, 16, 7981–8007, <https://doi.org/10.5194/acp-16-7981-2016>,
 850 2016.

851 Reimann, S. and Lewis, A. C.: Anthropogenic VOCs, in: *Volatile Organic Compounds in the Atmosphere*, edited by:
 852 Koppmann, R., Blackwell Publishing Ltd, <https://doi.org/10.1002/9780470988657>, 2007.

853 Richters, S., Herrmann, H., and Berndt, T.: Highly Oxidized RO₂ Radicals and Consecutive Products from the
 854 Ozonolysis of Three Sesquiterpenes, *Environ. Sci. Technol.*, 50, 2354–2362, <https://doi.org/10.1021/acs.est.5b05321>,
 855 2016.

856 Saarikoski, S., Hellén, H., Praplan, A. P., Schallhart, S., Clusius, P., Niemi, J. V., Kousa, A., Tykkä, T., Kouznetsov, R.,
 857 Aurela, M., Salo, L., Rönkkö, T., Barreira, L. M. F., Pirjola, L., and Timonen, H.: Characterization of volatile organic
 858 compounds and submicron organic aerosol in a traffic environment, *Atmos. Chem. Phys.*, 23, 2963–2982,
 859 <https://doi.org/10.5194/ACP-23-2963-2023>, 2023.

860 Seinfeld, J. H. and Pandis, S. N.: *Atmospheric Chemistry and Physics: From Air Pollution to Climate Change*, Third
 861 edit., Hoboken, New Jersey : John Wiley & Sons, Inc., ISBN 978-1-118-94740-1, 2016.

862 Shen, H., Zhao, D., Pullinen, I., Kang, S., Vereecken, L., Fuchs, H., Acir, I. H., Tillmann, R., Rohrer, F., Wildt, J.,
 863 Kiendler-Scharr, A., Wahner, A., and Mentel, T. F.: Highly Oxygenated Organic Nitrates Formed from NO₃Radical-
 864 Initiated Oxidation of β -Pinene, *Environ. Sci. Technol.*, 55, 15658–15671, <https://doi.org/10.1021/acs.est.1c03978>,
 865 2021.

866 Timonen, H., Karjalainen, P., Saukko, E., Saarikoski, S., Aakko-Saksa, P., Simonen, P., Murtonen, T., Dal Maso, M.,
 867 Kuuluvainen, H., Bloss, M., Ahlberg, E., Svenningsson, B., Pagels, J., Brune, W. H., Keskinen, J., Worsnop, D. R.,
 868 Hillamo, R., and Rönkkö, T.: Influence of fuel ethanol content on primary emissions and secondary aerosol formation
 869 potential for a modern flex-fuel gasoline vehicle, *Atmos. Chem. Phys.*, 17, 5311–5329, <https://doi.org/10.5194/ACP-17-5311-2017>, 2017.

871 Valiev, R. R., Hasan, G., Salo, V. T., Kubečka, J., and Kurten, T.: Intersystem Crossings Drive Atmospheric Gas-Phase
 872 Dimer Formation, *J. Phys. Chem. A*, 123, 6596–6604, <https://doi.org/10.1021/acs.jpca.9b02559>, 2019.

873 Wang, Z., Ehn, M., Rissanen, M. P., Garmash, O., Quéléver, L., Xing, L., Monge-Palacios, M., Rantala, P., Donahue,
 874 N. M., Berndt, T., and Sarathy, S. M.: Efficient alkane oxidation under combustion engine and atmospheric conditions,
 875 *Commun. Chem.* 2021 41, 4, 1–8, <https://doi.org/10.1038/s42004-020-00445-3>, 2021.

876 Watson, J. G., Chow, J. C., and Fujita, E. M.: Review of volatile organic compound source apportionment by chemical
 877 mass balance, *Atmos. Environ.*, 35, 1567–1584, [https://doi.org/10.1016/S1352-2310\(00\)00461-1](https://doi.org/10.1016/S1352-2310(00)00461-1), 2001.

Wayne, R. P.: Chemistry of atmospheres : an introduction to the chemistry of the atmospheres of earth, the planets, and their satellites, 3rd ed., Oxford : Oxford University Press, ISBN 978-0-19-850375-0, 2000.

Wayne, R. P., Barnes, I., Biggs, P., Burrows, J. P., Canosa-Mas, C. E., Hjorth, J., Le Bras, G., Moortgat, G. K., Perner, D., Poulet, G., Restelli, G., and Sidebottom, H.: The nitrate radical: Physics, chemistry, and the atmosphere, *Atmos. Environ. Part A, Gen. Top.*, 25, 1–203, [https://doi.org/10.1016/0960-1686\(91\)90192-A](https://doi.org/10.1016/0960-1686(91)90192-A), 1991.

WHO: WHO global air quality guidelines: particulate matter (PM_{2.5} and PM₁₀), ozone, nitrogen dioxide, sulfur dioxide and carbon monoxide, <https://apps.who.int/iris/handle/10665/345329>, last access: 30 August 2023, 2021.

Yan, C., Nie, W., Aijälä, M., Rissanen, M. P., Canagaratna, M. R., Massoli, P., Junninen, H., Jokinen, T., Sarnela, N., Häme, S. A. K., Schobesberger, S., Canonaco, F., Yao, L., Prévôt, A. S. H., Petäjä, T., Kulmala, M., Sipilä, M., Worsnop, D. R., and Ehn, M.: Source characterization of highly oxidized multifunctional compounds in a boreal forest environment using positive matrix factorization, *Atmos. Chem. Phys.*, 16, 12715–12731, <https://doi.org/10.5194/acp-16-12715-2016>, 2016.

Yan, C., Nie, W., Vogel, A. L., Dada, L., Lehtipalo, K., Stolzenburg, D., Wagner, R., Rissanen, M. P., Xiao, M., Ahonen, L., Fischer, L., Rose, C., Bianchi, F., Gordon, H., Simon, M., Heinritzi, M., Garmash, O., Roldin, P., Dias, A., Ye, P., Hofbauer, V., Amorim, A., Bauer, P. S., Bergen, A., Bernhammer, A. K., Breitenlechner, M., Brilke, S., Buchholz, A., Mazon, S. B., Canagaratna, M. R., Chen, X., Ding, A., Dommen, J., Draper, D. C., Duplissy, J., Frege, C., Heyn, C., Guida, R., Hakala, J., Heikkinen, L., Hoyle, C. R., Jokinen, T., Kangasluoma, J., Kirkby, J., Kontkanen, J., Kürten, A., Lawler, M. J., Mai, H., Mathot, S., Mauldin, R. L., Molteni, U., Nichman, L., Nieminen, T., Nowak, J., Ojdanic, A., Onnela, A., Pajunaja, A., Petäjä, T., Piel, F., Quéléver, L. L. J., Sarnela, N., Schallhart, S., Sengupta, K., Sipilä, M., Tomé, A., Tröstl, J., Väisänen, O., Wagner, A. C., Ylisirniö, A., Zha, Q., Baltensperger, U., Carslaw, K. S., Curtius, J., Flagan, R. C., Hansel, A., Riipinen, I., Smith, J. N., Virtanen, A., Winkler, P. M., Donahue, N. M., Kerminen, V. M., Kulmala, M., Ehn, M., Worsnop, D. R., Voge, A. L., Dada, L., Lehtipä, K., Stolzenburg, D., Wagner, R., Rissanen, M. P., Xiao, M., Ahonen, L., Fischer, L., Rose, C., Bianchi, F., Gordon, H., Simon, M., Heinritzi, M., Garmash, O., et al.: Size-dependent influence of nox on the growth rates of organic aerosol particles, *Sci. Adv.*, 6, 4945–4972, <https://doi.org/10.1126/sciadv.aay4945>, 2020.

Yan, C., Shen, Y., Stolzenburg, D., Dada, L., Qi, X., Hakala, S., Sundström, A.-M., Guo, Y., Lipponen, A., Kokkonen, T. V., Kontkanen, J., Cai, R., Cai, J., Chan, T., Chen, L., Chu, B., Deng, C., Du, W., Fan, X., He, X.-C., Kangasluoma, J., Kujansuu, J., Kurppa, M., Li, C., Li, Y., Lin, Z., Liu, Y., Liu, Y., Lu, Y., Nie, W., Pulliainen, J., Qiao, X., Wang, Y., Wen, Y., Wu, Y., Yang, G., Yao, L., Yin, R., Zhang, G., Zhang, S., Zheng, F., Zhou, Y., Arola, A., Tamminen, J., Paasonen, P., Sun, Y., Wang, L., Donahue, N. M., Liu, Y., Bianchi, F., Daellenbach, K. R., Worsnop, D. R., Kerminen, V.-M., Petäjä, T., Ding, A., Jiang, J., and Kulmala, M.: The effect of COVID-19 restrictions on atmospheric new particle formation in Beijing, *Atmos. Chem. Phys.*, 22, 12207–12220, <https://doi.org/10.5194/ACP-22-12207-2022>, 2022.

Zha, Q., Yan, C., Junninen, H., Riva, M., Sarnela, N., Aalto, J., Quéléver, L., Schallhart, S., Dada, L., Heikkinen, L., Peräkylä, O., Zou, J., Rose, C., Wang, Y., Mammarella, I., Katul, G., Vesala, T., Worsnop, D. R., Kulmala, M., Petäjä, T., Bianchi, F., and Ehn, M.: Vertical characterization of highly oxygenated molecules (HOMs) below and above a boreal forest canopy, *Atmos. Chem. Phys.*, 18, 17437–17450, <https://doi.org/10.5194/ACP-18-17437-2018>, 2018.

915 Zhang, Q., Jimenez, J. L., Canagaratna, M. R., Ulbrich, I. M., Ng, N. L., Worsnop, D. R., and Sun, Y.: Understanding
 916 atmospheric organic aerosols via factor analysis of aerosol mass spectrometry: A review, *Anal. Bioanal. Chem.*, 401,
 917 3045–3067, <https://doi.org/10.1007/s00216-011-5355-y>, 2011.

918 Zhang, Y., Peräkylä, O., Yan, C., Heikkinen, L., Äijälä, M., Daellenbach, K. R., Zha, Q., Riva, M., Garmash, O.,
 919 Junninen, H., Paatero, P., Worsnop, D., and Ehn, M.: A novel approach for simple statistical analysis of high-resolution
 920 mass spectra, *Atmos. Meas. Tech.*, 12, 3761–3776, <https://doi.org/10.5194/amt-12-3761-2019>, 2019.

921 Zhang, Y., Peräkylä, O., Yan, C., Heikkinen, L., Äijälä, M., Daellenbach, K. R., Zha, Q., Riva, M., Garmash, O.,
 922 Junninen, H., Paatero, P., Worsnop, D., and Ehn, M.: Insights into atmospheric oxidation processes by performing
 923 factor analyses on subranges of mass spectra, *Atmos. Chem. Phys.*, 20, 5945–5961, [https://doi.org/10.5194/acp-20-](https://doi.org/10.5194/acp-20-5945-2020)
 924 5945-2020, 2020.

925 Zhang, Y., Li, D., Ma, Y., Dubois, C., Wang, X., Perrier, S., Chen, H., Wang, H., Jing, S., Lu, Y., Lou, S., Yan, C., Nie,
 926 W., Chen, J., Huang, C., George, C., and Riva, M.: Field Detection of Highly Oxygenated Organic Molecules in
 927 Shanghai by Chemical Ionization-Orbitrap, *Environ. Sci. Technol.*, 56, 7608–7617,
 928 <https://doi.org/10.1021/acs.est.1c08346>, 2022.

929